2008

AN EVALUATION OF EARTHQUAKE GROUND-MOTION SITE EFFECTS AT TWO SITES UNDERLAIN BY DEEP SOILS IN WESTERN KENTUCKY

Jonathan Larry McIntyre
University of Kentucky

ABSTRACT OF THESIS

AN EVALUATION OF EARTHQUAKE GROUND-MOTION SITE EFFECTS AT TWO SITES UNDERLAIN BY DEEP SOILS IN WESTERN KENTUCKY

Six earthquake acceleration time histories were used to evaluate the ground-motion response of two sites, VSAP and VSAS, near the New Madrid Seismic Zone. These earthquakes ranged in magnitude from M_w 3.6 to M_w 5.2 and were located 46 to 173 km away from the recording instruments. These two sites are underlain by thick sequences (100 and 590 m) of unlithified soil that have been shown to greatly influence earthquake ground motions.

Near-surface soil dynamic properties were characterized at the two sites using seismic SH-wave refraction, P-S suspension logging, borehole electrical logs, and geotechnical logging methods. The soil properties were developed into a soil model for each site and the soil models were used to compare theoretical ground-motion models to the actual strong-motion time histories. An 1-D ground-motion simulation program (EERA) was used to complete the theoretical ground-motion analysis.

The results of the model indicated that the soils underlying VSAP generated amplification factors of 0.9 to 2.9 at about 6 and 9 Hz. Soils underlying VSAS generated amplification factors of 1.8 to 4.2 at about 5 Hz. These values correlated well with the observations at the two sites.

KEYWORDS: Amplification Factor, New Madrid, Suspension Logging, EERA, Site Effects

Jonathan Larry McIntyre

12-12-08

AN EVALUATION OF EARTHQUAKE GROUND-MOTION SITE EFFECTS AT TWO SITES UNDERLAIN BY DEEP SOILS IN WESTERN KENTUCKY

By

Jonathan Larry McIntyre

Dr. Edward W. Woolery

Director of Thesis

Dr. Dhananjay Ravat

Director of Graduate Studies

RULES FOR USE OF THESES

Unpublished theses submitted for the Master's degree and deposited in the University of Kentucky Library are as a rule open for inspection, but are to be used only with due regard to the rights of the authors. Bibliographical references may be noted, but quotations or summaries of parts may be published only with permission of the author, and with the usual scholarly acknowledgments.

Extensive copying or publication of the thesis in whole or in part also requires the consent of the Dean of the Graduate School of the University of Kentucky.

A library that borrows this thesis for use by its patrons is expected to secure the signature of each user.

Name	Date

THESIS

Jonathan Larry McIntyre

The Graduate School

University of Kentucky

2008

AN EVALUATION OF EARTHQUAKE GROUND-MOTION SITE EFFECTS AT TWO SITES UNDERLAIN BY DEEP SOILS IN WESTERN KENTUCKY

THESIS

A thesis submitted in partial fulfillment of the
requirements for the degree of Master of Science in the
College of Arts and Sciences
at the University of Kentucky

By

Jonathan Larry McIntyre

Lexington, Kentucky

Director: Dr. Edward W. Woolery, Professor of Geophysics

Lexington, Kentucky

2008

ACKNOWLEDGMENTS

I would like to give great acknowledgement to Dr. Edward W. Woolery, Dr. Zhenming Wang, and Dr. William A. Thomas for the direction and time contributed to this project. I would particularly like to thank Dr. Wooler and Dr. Wang for their valuable critiques, guidance and instruction. I would also like to thank Dr. Ron Street for his contribution and guidance in my education.

TABLE OF CONTENTS

LIST OF TABLES

LIST OF FIGURES

LIST OF FILES

File1, McIntyreThesis.PDF, 5.4 MB (CD)

CHAPTER ONE

1. INTRODUCTION

The New Madrid Seismic Zone is the most seismically active region in the central and eastern United States (Fig. 1). At least three large earthquakes (M > 7.0) have occurred along the New Madrid faults between winter 1811 and spring 1812 (Nuttli, 1973; Johnston and Schweig, 1996; Hough et al., 2000; Bakun et al., 2003). Paleo-liquefaction records (Tuttle et al., 2002) suggest that large earthquakes similar to the 1811-12 events have occurred twice in the past 1,200 years in the New Madrid Seismic Zone. Although the causes of these large intraplate earthquakes are not well understood, they pose certain hazards and risks because of their proximities to population centers such as Memphis, Tenn., and St. Louis, Mo., which are located on thick sequences of unlithified sediment.

The local and near-surface geology can influence site ground motions during an earthquake. The most prominent site effect is amplification of earthquake ground motions in areas underlain by a thick sequence of sediments. The classic site effect example is the 1985 M 8.1 Michoacan earthquake that resulted in catastrophic consequences for Mexico City, located approximately 350 km from the earthquake hypocenter. Singh et al. (1988) found that ground motions at sites in Mexico City underlain by lake bed deposits (10- to 80-meter-thick deposits of soft clay with a high water content) appeared to be amplified up to 75 times compared to hard-rock coastal sites at equal distances from the earthquake hypocenter. Another example is the 1980 Sharpsburg earthquake (M 5.3) in Bath County, Ky. Figure 2 shows the modified Mercalli intensity (MMI) distribution from the

Sharpsburg earthquake (Hanson et al., 1980). As shown in Figure 2, much higher MMI, VII, was observed in downtown Maysville during the Sharpsburg earthquake. Lin (2003) found that the observed higher MMI in downtown Maysville is due to site amplification by the Ohio River soft alluvium. Street et al. (1988) and Zhang et al. (1993) also found that ground motion from the $m_{b,Lg}$ 4.9 June 10, 1987, southern Illinois earthquake was amplified by as much as 4.8 times peak acceleration.

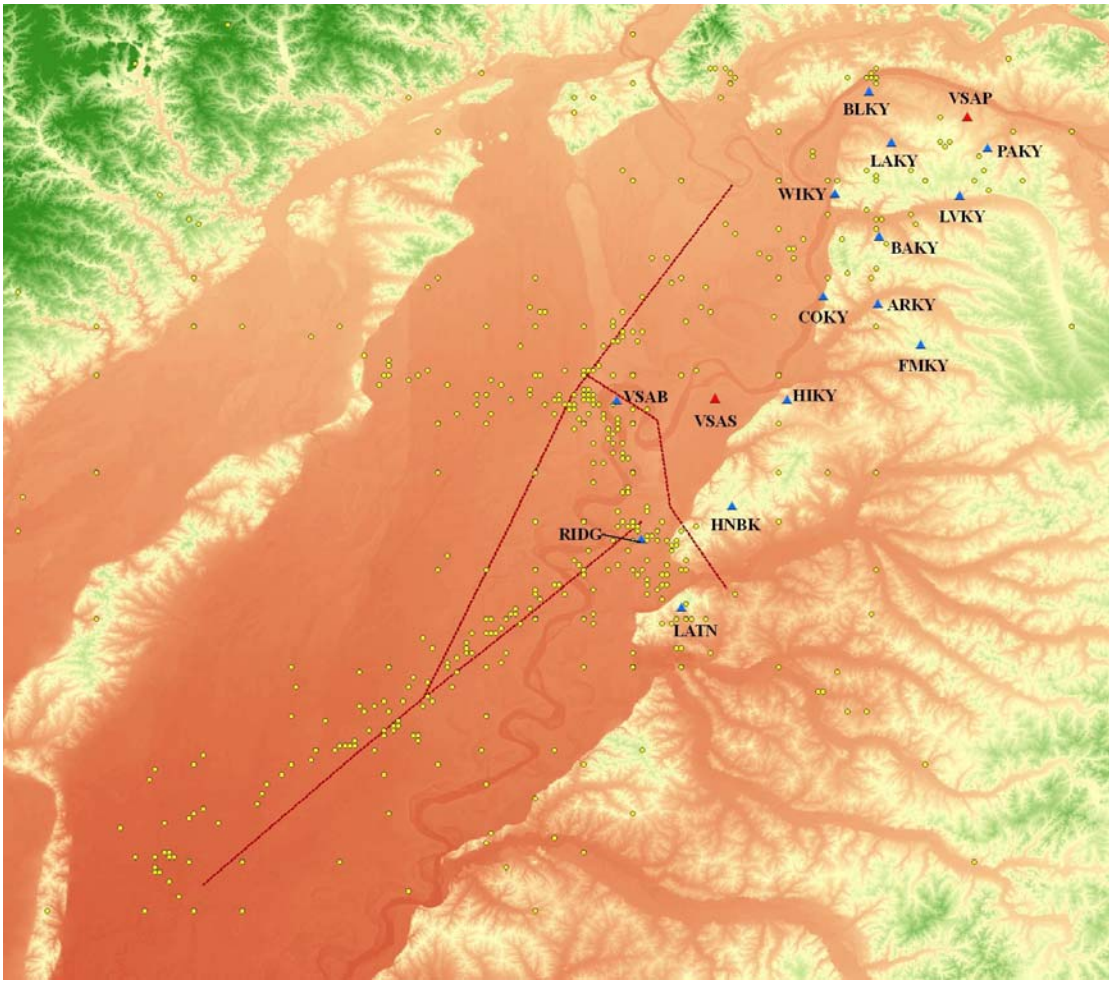

Figure 1. New Madrid Seismic Zone and the Kentucky Seismic and Strong-Motion Network.

Figure 2. Modified Mercalli intensity (MMI) distribution from the 1980 Sharpsburg earthquake (M 5.3) in Bath County, Ky. (Hanson et al., 1980).

Since the 1990's, the University of Kentucky has installed and operated a strong-motion network in northeastern part of the New Madrid Seismic Zone (Fig. 1). A unique feature of the network is the inclusion of vertical strong-motion arrays, each with one or two downhole accelerometers. The first vertical strong-motion recording in the central and eastern United States was made at station VSAP from the February 5, 1994, southern Illinois earthquake (Street et al., 1997). The deepest borehole array is 260 m below the surface at station VSAS in Fulton County, Ky. (Fig. 1). The vertical accelerometer array

at VSAS consists of three three-component accelerometers, recorded on a 24-bit, 12-channel K2 digital recorder equipped with GPS timing. The deep accelerometer (FBA-23DH) is at the bottom of the borehole. The second (ES-152DH) is at the bottom of a 30 m geotechnical hole. The third (EpiSensor®) is a free-field surface installation. The Kentucky Strong-Motion Network has recorded more than 200 earthquakes with magnitudes ranging from 1.5 to 5.2 $m_{b,Lg}$ (Street and Wang, 2003; Wang et al., 2003; Wang and Woolery, 2006). The vertical strong-motion arrays operated by the University of Kentucky have accumulated recordings that will provide a database for scientists and engineers to study the effects of the near-surface soils on the strong ground motion in the New Madrid Seismic Zone.

1.1. Purpose and Significance

This study assesses the site effects at two sites (VSAP and VSAS) located near the New Madrid Seismic Zone in the western Kentucky portion of the Upper Mississippi Embayment, where thick Cretaceous to recent unlithified sediments overlie Paleozoic bedrock (Fig. 1). Included is an evaluation of strong ground motions near seismogenic sources (< 200 km) for moderate-size earthquakes in the central United States, achieved by comparing theoretical models and predictive earthquake-induced ground motions in the region with strong-motion recordings from the vertical arrays of the Kentucky Seismic and Strong-Motion Network at the two sites. Soil models were developed using P- and S-wave seismic refraction and reflection data, along with borehole seismic velocity data and geotechnical data.

Two vertical strong-motion seismic arrays (VSAP, VSAS) are located at sites underlain by thick (> 100 m) sequences of unlithified sediment. These vertical strong-

motion arrays have provided data for evaluation of near-surface effects on seismic ground motion. Seismic wave amplification exposes several population centers (e.g., Memphis, Tenn., and St. Louis, Mo.) underlain by thick sediments near the New Madrid Seismic Zone to potentially significant risk.

Strong bedrock ground motions in the region are poorly recorded as a result of the infrequent occurrence of moderate and large earthquakes in the area, as well as the limited availability of bedrock outcrops/shallow bedrock sites; therefore, the actual effects of the deep soils on seismic ground motions are poorly understood. Results from this study can also serve as a calibration aid when analyzing strong-motion data for other sites in the region. This study is unique from previous site-effect studies in the New Madrid Seismic Zone because it compares actual seismic ground motions at the bedrock and the surface to theoretically derived synthetic ground motions.

CHAPTER TWO

2. SOIL MODEL

2.1. VSAP

VSAP is located on a thick sequence of unlithified to poorly lithified sands, clays, and gravels of Late Cretaceous to recent age that overlies Mississippian limestone bedrock of the Warsaw Formation (Harris, 1992). The surface of the limestone bedrock is irregular and exhibits karst geomorphology and represents an unconformity between rock and soil underlying the site. Pleistocene loess extends from the surface to a depth of 5 m below ground surface, as interpreted from seismic shear-wave (SH-wave) refraction data (Harris, 1992). The Pleistocene loess consists of at least three depositional formations; however, for the purposes of this study, the three loesses of the Loveland silt, Roxana silt, and Peoria loess are grouped together and will be referred to as Pleistocene loess. These deposits consist of clayey and sandy silts (Science Applications International Corporation, 2002).

The unconformity between the overlying Pleistocene loess and the underlying Continental Deposits is interpreted to be at approximately 5 m below the ground surface, utilizing SH-wave refraction data. The Continental Deposits range in age from Pleistocene, Pliocene, to possibly Miocene (Clausen et al., 1992). The Continental Deposits can be divided into the Lower Continental Deposits and the Upper Continental Deposits. The Lower Continental Deposits of the Mounds/Lafayette Gravel formation consist of sand and gravel of varying grain size and grading (Science Applications International Corporation, 2002). The Upper Continental Deposits consist of an unstratified fining-upward sequence of sand that is capped by a silty clay/clayey silt and a

layer of sand and gravel (Science Applications International Corporation, 2002). The sands and gravels of the Lower Continental Deposits provide a groundwater flowpath and serve as a regional aquifer that is widely contiguous throughout the region, known as the Regional Gravel aquifer. A contact is interpreted within the Continental Deposits at a depth of 12 m. This may or may not coincide with the stratigraphic contact between the Lower and Upper Continental Deposits. Total thickness of the Continental Deposits is interpreted to be about 45 m, utilizing the SH-wave refraction data. Another unconformity separates the Continental Deposits from the underlying Clayton/McNairy Formations. The Clayton/McNairy Formations at the site are composed of silty and clayey fine sand with interbeds of silt and clay (Science Applications International Corporation, 2002).

The contact between the overlying McNairy Formation and the underlying Mississippian bedrock of the Warsaw Formation is a highly eroded unconformity. The depth to the top of bedrock is 100 m below ground surface, as interpreted from SH-wave refraction profiles (Harris, 1992). A weathered rubble zone is encountered just above the bedrock surface, as the Warsaw Formation is widely known for its expression of karstic features.

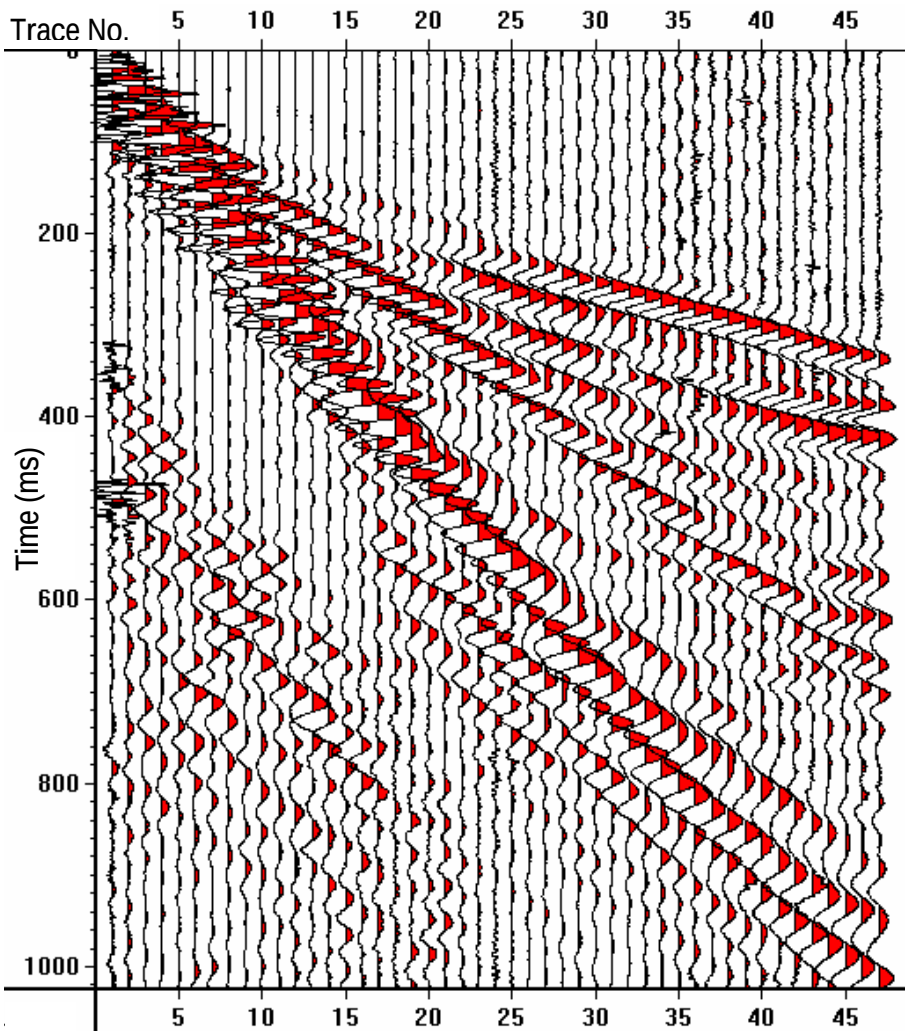

Figure 3. SH-wave refraction profile acquired at VSAP.

The soil model for VSAP was based on the velocity structure derived from two orthogonal SH-wave refraction profiles completed at the site. Figure 3 shows an SH-wave refraction profile collected at VSAP. The data were collected with 30-Hz geophones at a spacing of 4 m. The data were digitally sampled at a rate of 0.25 ms with an engineering seismograph. The SH-mode waves were generated by horizontal impacts of a 4.5-kg hammer to a steel H-pile section. To ensure the accurate identification of SH-mode events, impacts were recorded on opposite sides of the energy source oriented

perpendicular to the geophone spread. By striking each side of the source and reversing the acquisition polarity of the engineering seismograph, inadvertent P- and SV-mode energy was stacked in a destructive manner, while SH-mode energy was stacked constructively. Figures 4 and 5 show the shear-wave velocity structure of the subsurface down to bedrock at VSAP. Four soil layers and the bedrock were identified by the SH-wave refraction profiles and were incorporated into the soil model of VSAP (Fig. 6). The unit weights of the soil horizons were taken from Street et al. (1997). An additional soil horizon was added to the soil model in order to analyze the upper 30 m of soil.

In addition to the SH-wave refraction profiles, an SH-wave downhole survey was completed by Woolery and Wang (2005) at the site. The data from the downhole survey proved difficult to correlate to actual stratigraphic soil horizons, and it was determined that the refraction profiles would be better suited to the development of the soil model for VSAP.

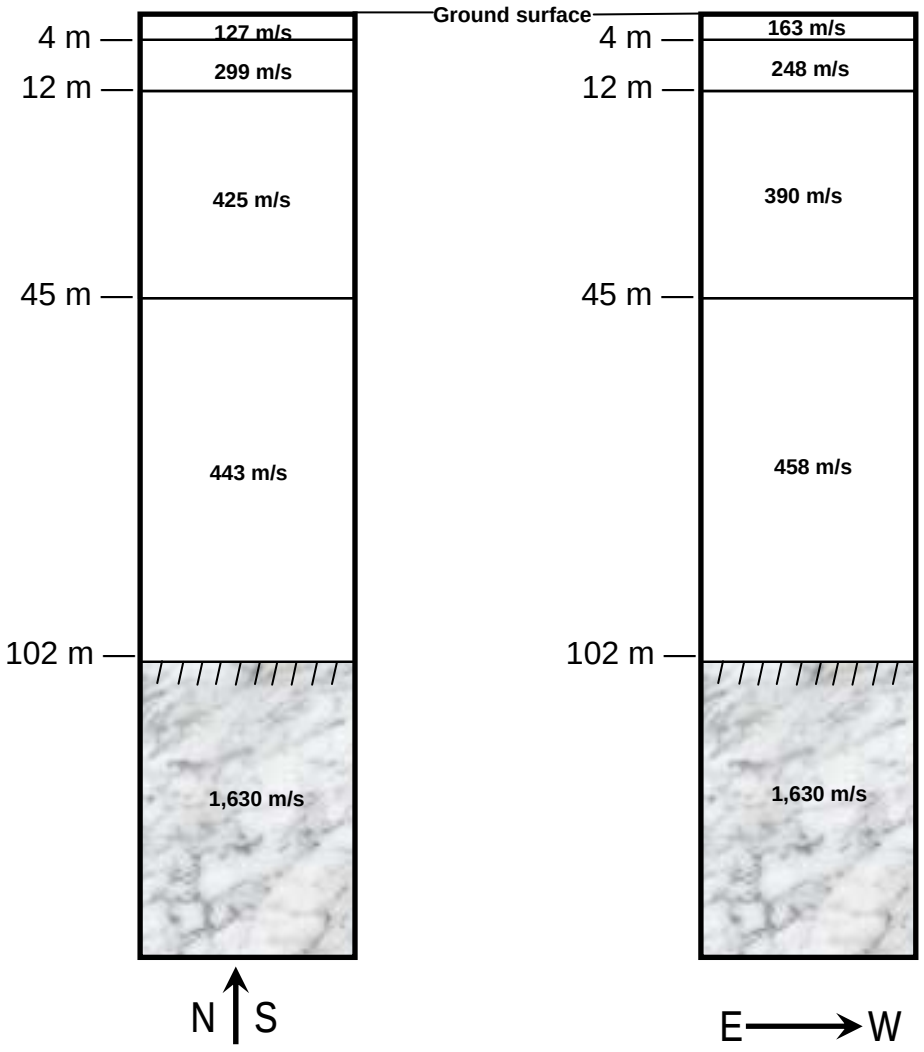

Figure 4. VSAP shear-wave velocity structure of the subsurface interpreted from SH-wave refraction profiles.

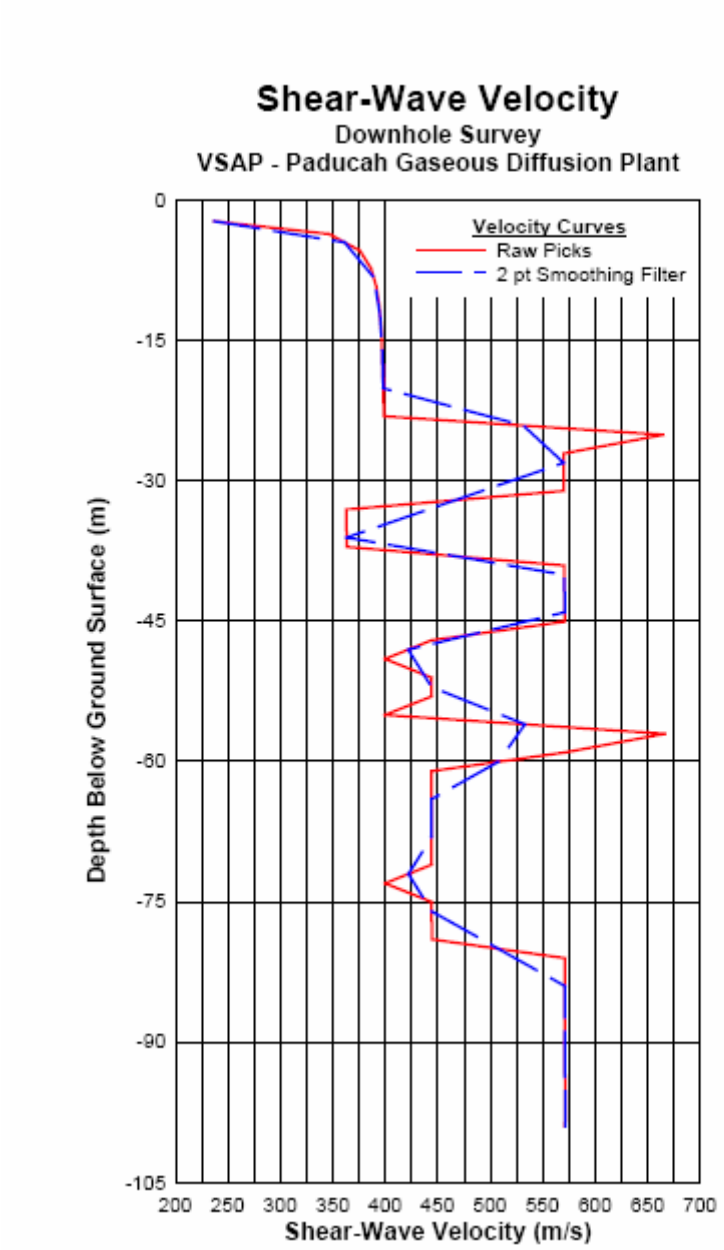

Figure 5. VSAP shear-wave velocity profile from a downhole test (Woolery and Wang, (2005).

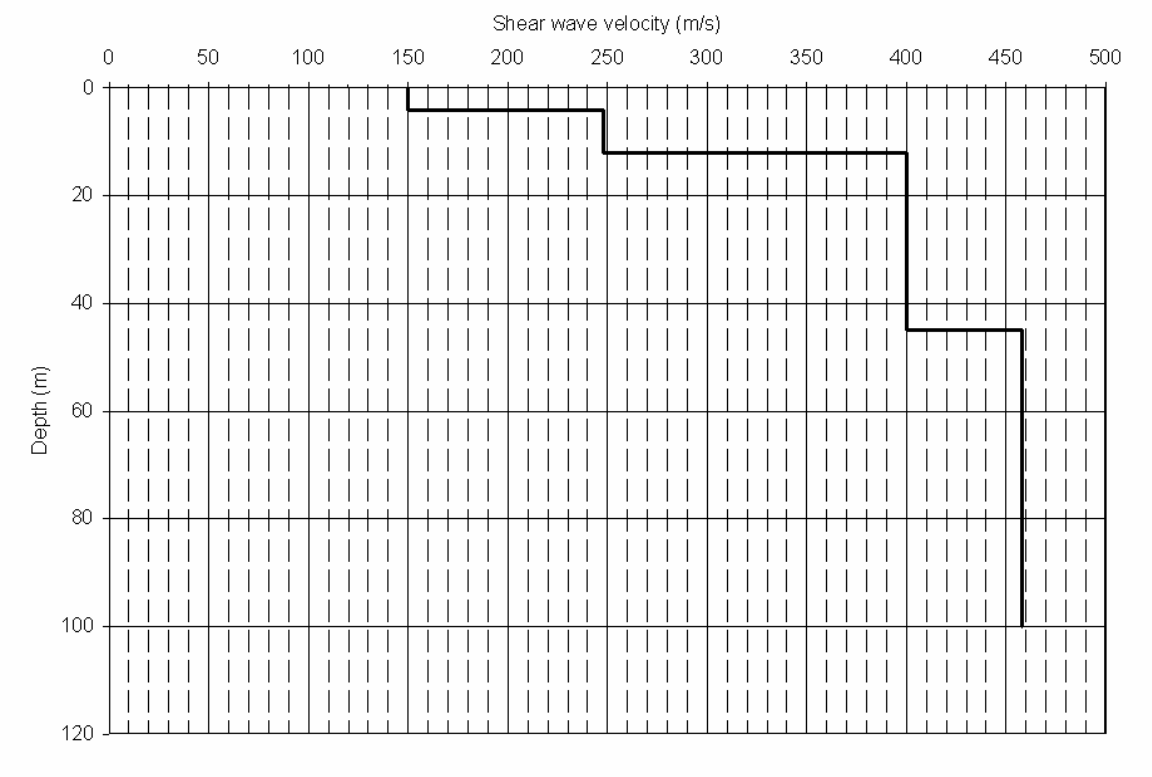

	Layer Number	Thickness of layer (m)	Maximum shear modulus G_{max} (MPa)	Total unit weight (kN/m^3)	Shear-wave velocity (m/sec)	Depth at middle of layer (m)	Vertical effective stress (kPa)
Surface	1	4.0	44.7	19.5	150	2.0	19.4
	2	8.0	122.3	19.5	248	8.0	77.5
	3	18.0	306.6	18.8	400	21.0	197.2
	4	15.0	306.6	18.8	400	37.5	345.5
	5	55.0	417.0	19.5	458	72.5	679.4
Bedrock	6		3787.2	25.8	1630	100.0	945.9

Figure 6. VSAP soil model.

2.2. VSAS

The site VSAS, like VSAP, is located on a thick sequence of unlithified to poorly lithified sands, clays, and gravels of Late Cretaceous to recent age that overlies Ordovician limestone bedrock. The surface of the limestone bedrock is irregular and exhibits karst geomorphology and represents an unconformity between rock and soil underlying the site. Depth to bedrock is about 590 m (Woolery and Wang, 2002).

The contact between the overlying alluvium at the surface and the underlying Jackson Formation is interpreted to be at about 50 m below the ground surface (Woolery and Wang, 2002). The contact between the overlying Jackson Formation and the underlying Claiborne Formation is placed approximately 130 m below the ground surface. The contact between the Claiborne Formation and the underlying Wilcox Formation is approximately 275 m below the ground surface. The contact between the Wilcox Formation and the underlying Porters Creek Clay is approximately 395 m below the ground surface. The Porters Creek Clay is a distinctive, thick sequence of clay in contrast to the sandy clay lithology of the Wilcox Formation. The contact between the Porters Creek Clay and the underlying Clayton and McNairy Formations is at approximately 485 m. The contact between the Clayton and McNairy Formations and Paleozoic bedrock is approximately 590 m below the ground surface.

A 594-m-deep borehole was drilled, cased, and logged at site VSAS in 2007. The 10.2-cm-diameter borehole extended approximately 10 m into the bedrock. Seismic suspension logging of both P-waves and shear waves was conducted at 1-m intervals from the surface to the bottom of the borehole. Figure 7 illustrates the P-S seismic suspension method. The OYO® P-S Logging System was utilized to conduct the

suspension log. The OYO® system uses a 7-m probe, containing a source and two receivers spaced 1 m apart, suspended by a cable. The armored four- or seven-conductor cable serves both to support the probe and to convey data to and from a recording/control device on the surface. The probe is lowered into the borehole to a specified depth (a rotary encoder on the winch measures probe depth), where the source generates a pressure wave in the borehole fluid. The pressure wave is converted to seismic waves (P and S) at the borehole wall. Along the wall at each receiver location, the P- and S-waves are converted back to pressure waves in the fluid and received by the geophones, which send the data to the recorder on the surface. The elapsed time between arrivals of the waves at the receivers is used to determine the average velocity of a 1-m-high column of soil around the borehole. Source-to-receiver analysis is also performed for quality assurance. Many more soil layers were interpreted from the stratigraphic log (Fig. 8) than from the suspension log (Fig. 9). Twelve velocity layers were interpreted from the suspension log. The stratigraphic log was used primarily for determining the unit weight of the soil layers (i.e., determining clay and sand content and using the unit weights provided by Street. et al. [1997] for similar soil horizons). The seismic suspension, lithologic, gamma, resistivity, and spontaneous-potential logs were used to derive the soil model (Fig. 10), although the evaluation of the soil model was heavily weighted toward the interpretation of the shear-wave suspension log. Thirteen soil horizons were used in the soil model, although only 11 distinct soil horizons are interpreted in Figure 9. A soil layer was added as layer #2 to the soil model (Fig. 10) to help analyze the behavior of the upper 30 m of the soil column, which is of interest when using standard geotechnical techniques. Another soil horizon was added as layer #8 between depths of 260.0 m and

264.4 m, in order to allow input of the earthquake time history into the EERA model at the depth of the deeper accelerometer at VSAP.

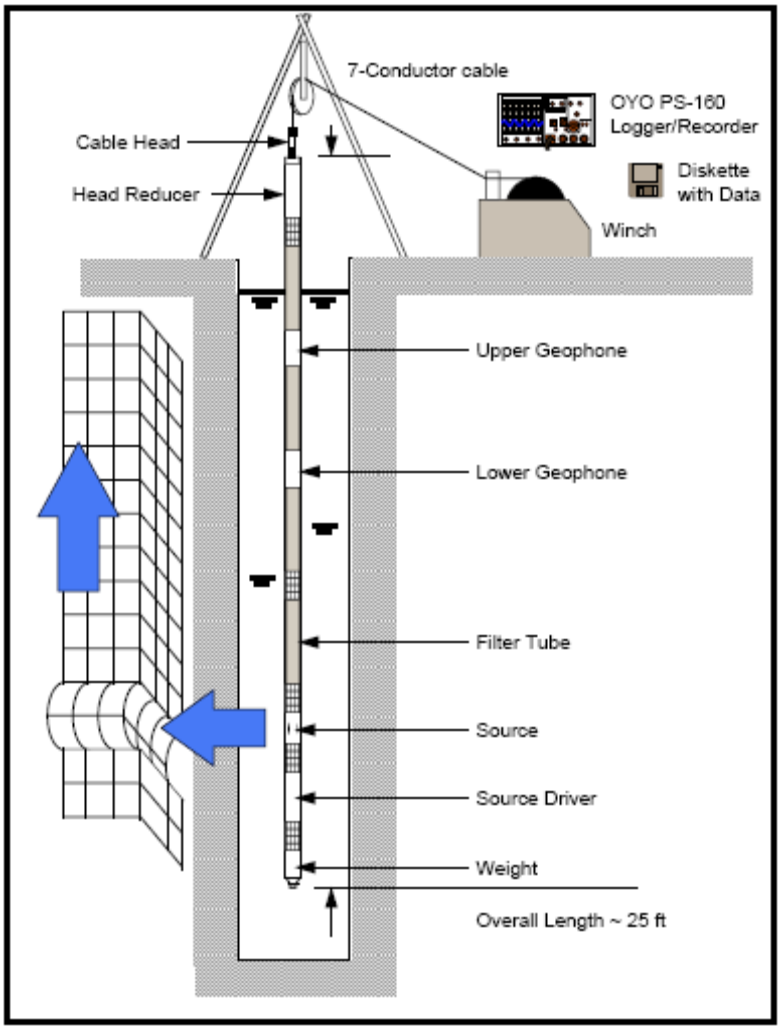

Figure 7. Illustration of P-S suspension logging method.

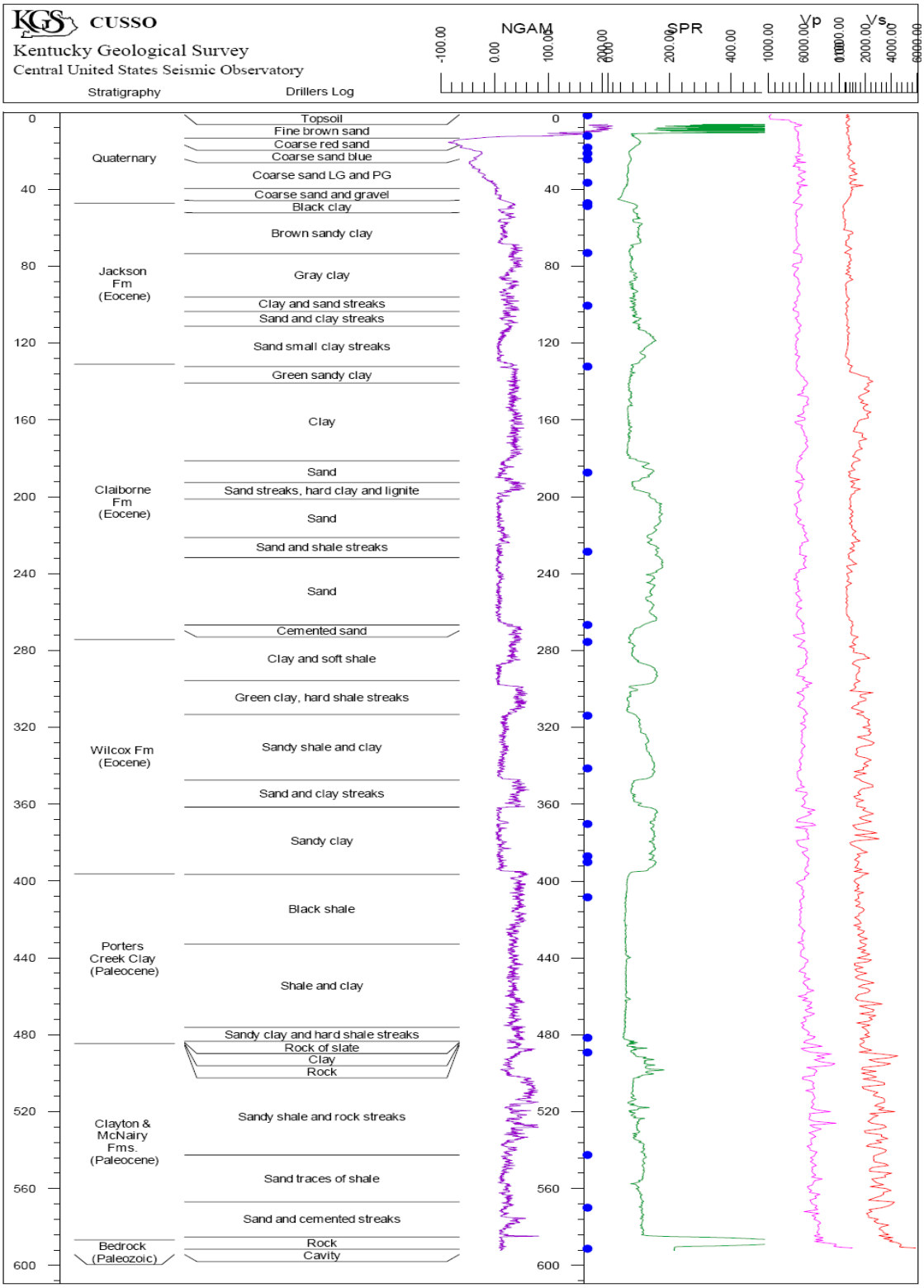

Figure 8. Stratigraphic/lithologic log of site VSAS. Geophysical logging of the borehole included on the log is gamma, spontaneous-potential, and seismic velocity.

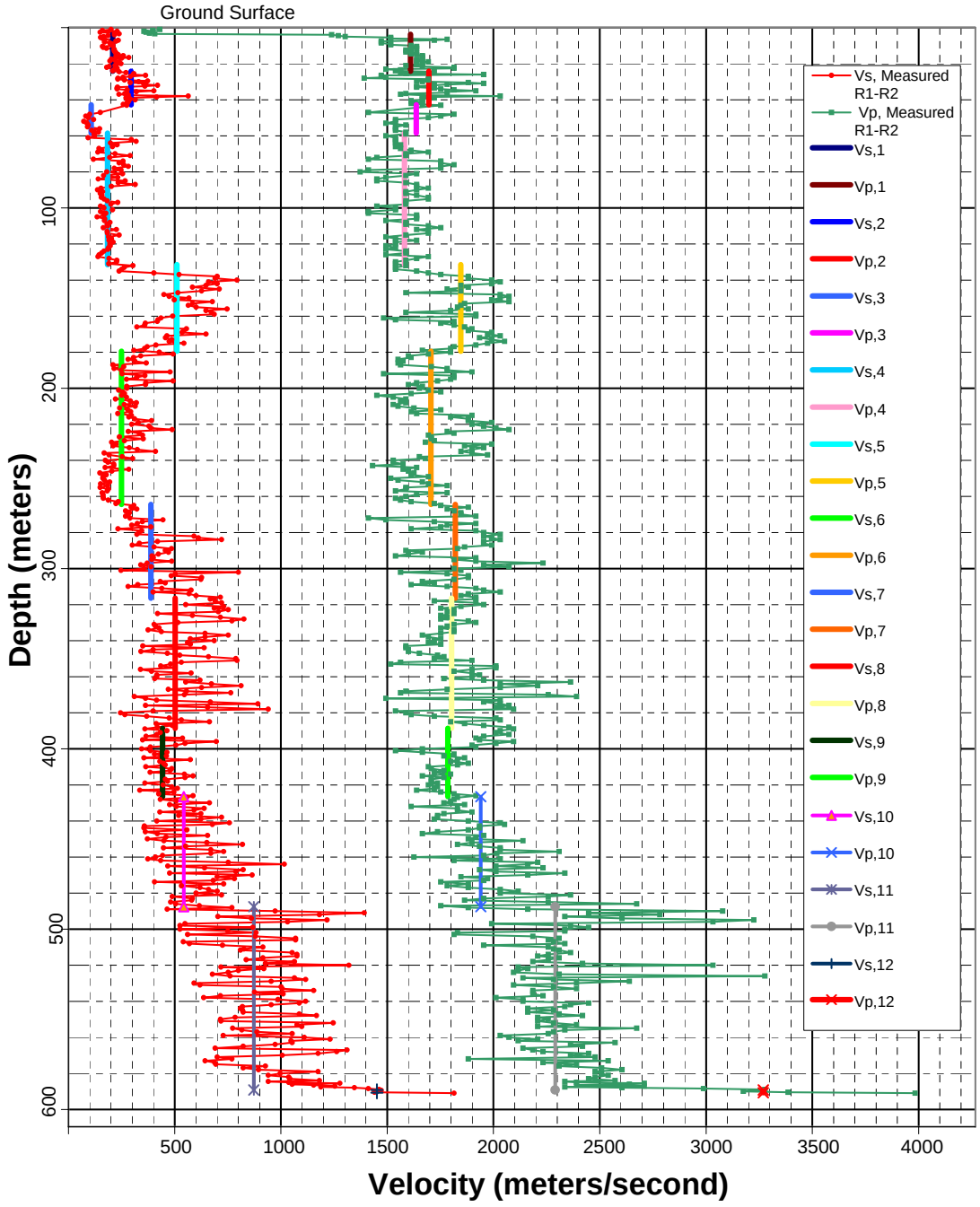

Figure 9. Shear-wave and P-wave velocity structure of the subsurface at site VSAS. The red data set represents shear-wave velocity with respect to depth. The green data set represents P-wave velocity with respect to depth. Interpreted velocity horizons are identified in the legend.

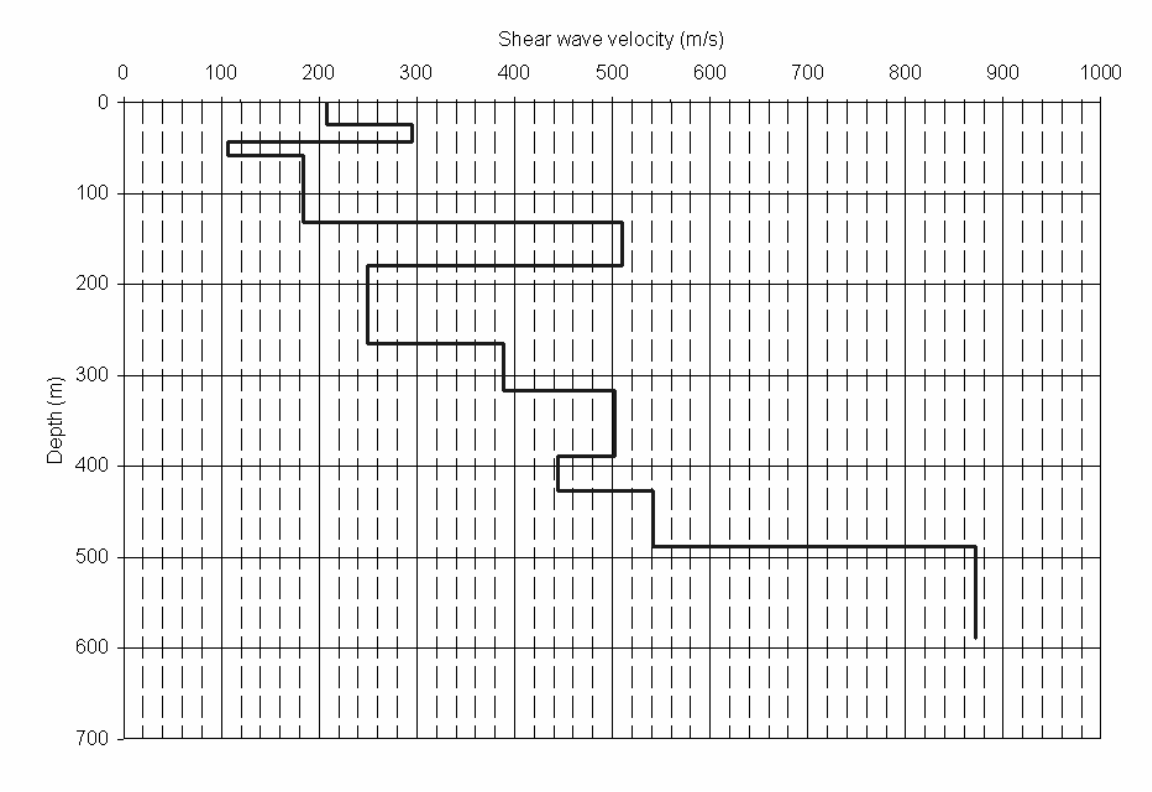

	Layer Number	Thickness of layer (m)	Maximum shear modulus G_{max} (MPa)	Total unit weight (kN/m^3)	Shear wave velocity (m/sec)	Depth at middle of layer (m)	Vertical effective stress (kPa)
Surface	1	24.2	82.9	18.8	208	12.1	108.8
	2	5.8	166.8	19.5	295	27.1	243.6
	3	12.7	173.0	19.5	295	36.4	331.7
	4	15.7	22.8	19.5	107	50.7	469.8
	5	73.0	67.3	19.5	184	95.0	899.6
	6	48.0	517.0	19.5	510	155.5	1485.8
	7	80.6	119.8	18.8	250	219.8	2080.7
	8	4.4	119.8	18.8	250	262.3	2462.7
	9	52.0	299.25	19.5	388	290.5	2734.5
	10	72.0	500.9	19.5	502	352.5	3335.2
	11	38.0	391.9	19.5	444	407.5	3868.2
	12	61.0	583.9	19.5	542	457.0	4347.8
	13	101.7	1511.5	19.5	872	538.3	5136.1
Bedrock	14		5544.8	25.8	1452	589.2	5628.9

Figure 10. VSAS soil model.

CHAPTER THREE

3. SOIL RESPONSE ANALYSIS

The site response analyses were conducted using an equivalent-linear code, EERA (Bardet et al. 2000), which operates on the same basic concepts as SHAKE/SHAKE91 (Schnabel et al., 1972; Idriss and Sun, 1991). EERA was developed in FORTRAN 90 and is an acronym for equivalent-linear earthquake response analysis. EERA computes one-dimensional soil responses for a system of homogeneous, viscoelastic layers of infinite horizontal extent that are subjected to vertically traveling shear waves. The program uses a continuous solution to the wave equation adapted for use with transient motions through the fast Fourier transform algorithm. Nonlinearity of the shear modulus and damping are approximated by the use of equivalent linear soil properties and numerically obtaining values compatible with the effective strains in each layer. EERA computes the response in a horizontally layered soil-rock system subjected to transient and vertical traveling shear waves. EERA assumes that the cyclic soil behavior can be replicated using an equivalent linear model, an assumption that has been extensively described in the geotechnical earthquake engineering literature (e.g., Idriss and Seed, 1968; Seed and Idriss, 1970; Kramer, 1996).

EERA assumes simplified geometry and cyclic behavior of the materials. The specific basic assumptions follow Yule and Wahl (1996):

1. The soil horizons are horizontal and extend infinitely.
2. The ground surface is horizontal.
3. Each soil unit can be completely defined by the shear modulus, damping function, layer thickness, and unit weight. Values are frequency independent.

4. The nonlinear cyclic behavior is adequately characterized by the linear viscoelastic (Voigt) constitutive model and implemented with the equivalent linear method.
5. The incident earthquake motions are spatially uniform, horizontally polarized shear waves that are propagated vertically through the soil column.

The transfer function defines the relationship between the soil properties and the amplification factor; furthermore, the transfer function is regarded as a surface layer filter, thus a function of the soil layer properties such as damping ratio, layer thickness, shear modulus, unit weight, and seismic wave velocity. The transfer function converts the input bedrock motion to output soil motion. A schematic of the transfer function is shown in Figure 11. The transfer function in its simplest form can be written (Kramer, 1996):

$$S(\omega) = T(\omega)A(\omega) \tag{3-1}$$

$S(\omega)$ = response spectrum at that layer (typically free surface)

$A(\omega)$ = spectrum of the incident wave at the bottom of the soil column

$T(\omega)$ = transfer function defining the physical properties of the soil column

ω = the angular frequency of the wave motion, or $2\pi f$ (where f is frequency).

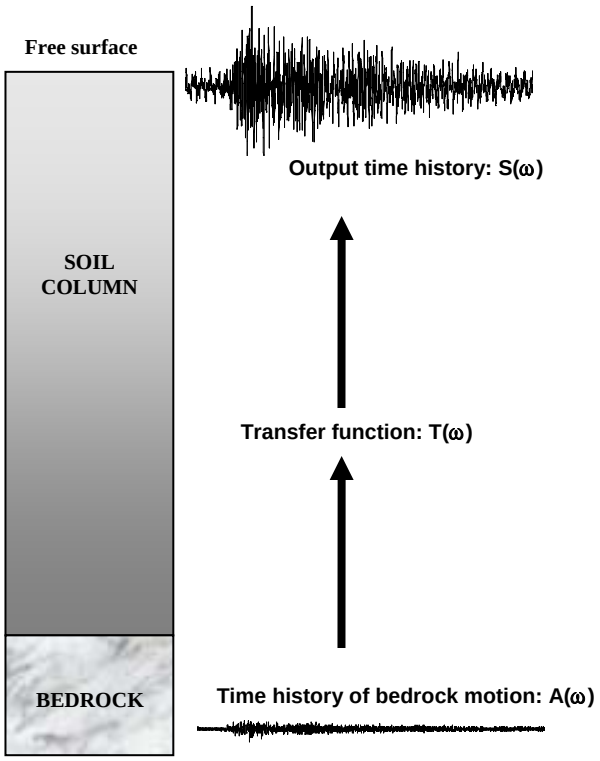

Figure 11. Illustration of the transfer function.

Kramer (1996) defined the transfer function :

$$T(\omega) = \frac{1}{\cos\left[\frac{\omega H}{V_s(1+i\xi)}\right]} \tag{3-2}$$

ξ = damping ratio, which is equal to $\frac{C}{C_c} = \frac{C\omega_0}{2k}$

C_c = critical damping coefficient

k = wave number

H = soil layer thickness

V_s = shear-wave velocity of the soil layer

Given that $\left|\cos(x+iy)\right| = \sqrt{\cos^2 x + \sinh^2 y}$ and $\sinh^2 y \approx y^2$, equation 3-2 can be expressed as:

$$\left|T(\omega)\right| = \frac{1}{\sqrt{\cos^2\left(\frac{\omega H}{V_s}\right) + \left[\xi\left(\frac{\omega H}{V_s}\right)\right]^2}} \tag{3-3a}$$

$$\left|T(f)\right| = \frac{1}{\sqrt{\cos^2\left(\frac{2\pi f H}{V_s}\right) + \left[\xi\left(\frac{2\pi f H}{V_s}\right)\right]^2}}. \tag{3-3b}$$

The n^{th} layer natural angular frequency can be written:

$$\omega_n = \frac{V_s}{H}\left(\frac{\pi}{2} + n\pi\right) \tag{3-4a}$$

$$f_n = \frac{V_s}{H}\left(\frac{2n+1}{4}\right). \tag{3-4b}$$

Combining Equations 2-3 and 2-4 results in:

$$\left|T(\omega)\right| \frac{1}{\sqrt{\cos^2\left(\omega\frac{\frac{\pi}{2}+n\pi}{\omega_n}\right) + \left[\xi\left(\omega\frac{\frac{\pi}{2}+n\pi}{\omega_n}\right)\right]^2}}. \tag{3-5}$$

$\left|T(\omega)\right|$ defines the local maximum value when $\omega_n \approx \omega$. As n increases, the local maximum value decreases due to damping effects of the soil column, and the largest amplification is found at $n = 0$. When $n = 0$ in equation 3-4, the n^{th} layer natural angular frequency is the fundamental frequency (f_0) of the soil column as defined by:

$$f_0 = \frac{V_s}{4H}. \tag{3-6}$$

It is intuitive to expect the maximum amplification of ground motions to occur near the fundamental frequency. Therefore, knowledge of the soil layer thicknesses is important for estimating the total site effect of the soil column on ground motions. The soil's shear-wave velocity structure influences the frequency at which maximum amplification occurs. Equations 3-5 and 3-3 define the relationship between the soil column properties and amplification of ground motions. Therefore, the transfer function may be viewed as a filter that acts upon some input signal to produce an output signal.

The procedure for Fourier analysis of a single degree of freedom system response can be summarized in the following steps:

1. Obtain the Fourier series for the applied loading (or base motion). In doing so, the loading is expressed as a function of frequency rather than a function of time.
2. Multiply the Fourier series coefficients by the appropriate value of the transfer function at each frequency, ω_n. This will produce the Fourier series of the output motion.
3. Express the output motion in the time domain by obtaining the inverse Fourier transform of the output motion.

For the ground response problem, transfer functions can be used to express various response parameters, such as displacement, velocity, acceleration, shear stress, and shear strain, to an input motion parameter such as bedrock acceleration. Because it relies on the principle of superposition, this approach is limited to the analysis of linear systems. Nonlinear behavior can be approximated, however, using an iterative procedure

with equivalent linear soil properties. A known time history of bedrock (input) motion is represented as a Fourier series, usually using the fast Fourier transform. Each term in the Fourier series of the bedrock (input) motion is then multiplied by the transfer function to produce the Fourier series of the ground surface (output) motion. The ground surface (output) motion can then be expressed in the time domain using the inverse fast Fourier transform. Thus, the transfer function determines how each frequency in the bedrock (input) motion is amplified or deamplified by the soil column.

The key to the linear approach to ground response analysis is the evaluation of transfer functions. The linear approach requires that G and ξ be constant for each soil layer. The problem then becomes one of determining the values that are consistent with the level of strain induced in each layer. To address the problem, an objective definition of strain level is needed.

Since computed strain level depends on the values of the equivalent linear properties, an iterative procedure is required to ensure that the properties used in the analysis are compatible with the computed strain levels in all layers. The iterative procedure operates as follows:

1. Initial estimates of G and ξ are made for each layer. The initially estimated values usually correspond to the same stain level; the low-strain values are often used for the initial estimate.
2. The estimated G and ξ values are used to compute the ground response, including time histories of shear strain for each layer.
3. The effective shear strain in each layer is determined from the maximum shear strain in the computed shear strain time history.

4. From this effective shear strain, new equivalent linear values, G and ξ, are chosen for the next iteration.
5. Steps 2 to 4 are repeated until differences between the computed shear modulus and damping ratio values in two successive iterations fall below some predetermined value in all layers. Although convergence is not absolutely guaranteed, differences of less than 5 to 10 percent are usually achieved in three to five iterations (Schnabel et al., 1972).

Because the equivalent linear approach utilizes a linear analysis, the response at any point can be related to the response at any other point. Although the transfer functions are related to the computation of free-surface motion from bedrock motion, transfer functions relating motions at other depths can also be derived without difficulty.

CHAPTER FOUR

4. RESULTS

4.1. Strong-Motion Data

Acceleration time histories for six earthquakes were utilized for the comparative study. These earthquakes ranged in magnitude between M_w 3.6 and M_w 5.2, and epicentral distances between 46 km and 173 km. Specific details for the individual earthquakes follow:

1. April 18, 2008. Southern Illinois. M_w 5.2.
   Latitude: 38.450 N
   Longitude: 87.890 W
   Depth: 11.6 km

2. April 18, 2008. Southern Illinois. M_w 4.6.
   Latitude: 38.478 N
   Longitude: 87.869 W
   Depth: 10.0 km

3. February 10, 2005. Northeastern Arkansas. M_w 4.1.
   Latitude: 35.760 N
   Longitude: 90.250 W
   Depth: 15.5 km

4. April, 21, 2008. Southern Illinois. M_w 4.0.
   Latitude: 38.491 N
   Longitude: 87.863 W
   Depth: 10.0 km

5. June 2, 2005. Ridgely, Tenn. M_w 3.9.
   Latitude: 36.150 N
   Longitude: 89.470 W
   Depth: 15.1 km

6. June 20, 2006. Blandville, Ky. M_w 3.6.
   Latitude: 36.920 N
   Longitude: 89.000 W
   Depth: 8.9 km

Acceleration time histories for these events were recorded using three-component force-balanced accelerometers and Kinemetrics K2® accelographs maintained by the University of Kentucky/Kentucky Geological Survey. The seismic instrumentation at VSAP consists of a three-component downhole Kinemetrics FBA-13DH accelerometer, a three-component free-field Kinemetrics EpiSensor® accelerometer, and a Mark Products L-4C short-period seismometer. Strong-motion seismic records are recorded with a 24-bit Kinemetrics K2® 12-channel digital accelograph. Weak-motion seismic records are recorded with a 24-bit NetDAS® digital data acquisition system. The FBA-13 DH accelerometer is located at the soil-rock interface at a depth of 100 m below the ground surface.

The seismic instrumentation at VSAS consists of a three-component Kinemetrics FBA-23DH accelerometer, a three-component ES-152DH, accelerometer and a three-component free-field Kinemetrics EpiSensor® accelerometer. Strong-motion data are recorded with a 24-bit Kinemetrics K2® 12-channel accelograph. The downhole accelerometers at VSAS are located 30 m and 260 m below the ground surface. The subsurface locations of these accelerometers were chosen for specific purposes. The depth of 30 m was chosen so that the behavior of strong ground motions could be evaluated exclusively in the upper 30 m of the soil column. Physical parameters of the upper 30 m of soil are routinely used in geotechnical engineering when evaluating earthquake site effects. By placing accelerometers at a depth of 30 m and at the surface, a more precise evaluation of seismic ground-motion site effects can be performed and compared to the estimated ground-motion site effects resulting from standard geotechnical investigations.

The sampling rate of the digitizers (K2) is 200 ms. The EpiSensor® and FBA accelerometers have a bandwidth of DC to 200 Hz. The maximum acceleration range of the EpiSensor® accelerometer is 1 G. The maximum acceleration of the FBA accelerometers is 0.25 G.

Acceleration time histories from the free-field accelerometer and the 100-m accelerometer (at the soil-rock interface) for VSAP were used. Time histories from the April 18, 2008, and April 21, 2008, southern Illinois events and the June 2, 2005, Ridgely, Tenn., event were the comparative earthquakes used for input ground motions at VSAP.

The time histories from the free-field accelerometer and the 260-m-deep accelerometer were used for VSAS. Time histories from the June 2, 2005, Ridgely, Tenn., event, the February 10, 2005, northeastern Arkansas event, and the June 20, 2006, Blandville, Ky., event were the comparative earthquakes used for input ground motions at site VSAS.

4.2. EERA Analysis

As discussed in chapter 3, ground motion at free surface can be calculated from the soil model and given input motion in bedrock. Figure 12 shows the input motion in bedrock (a) and output ground motion at free surface (b) at VSAP for the April 18, 2008, southern Illinois earthquake (M_w 5.2). Figure 13 shows the transfer function for this input bedrock motion at VSAP. In comparison, Figure 14 shows the spectral ratio between free-surface and bedrock recordings from the April 18, 2008, southern Illinois earthquake. As shown in Figure 12, ground motion is amplified through the soil column at VSAP.

Figure 15 shows the input motion in bedrock (a) and output ground motion at free surface (b) at VSAS for the June 20, 2005, Ridgely, Tenn., earthquake. Figure 16 shows the transfer function for this input bedrock motion at VSAS. Figure 17 shows the spectral ratio between free-surface and bedrock recordings from the June 20, 2005, Ridgely, Tenn., earthquake. As shown in Figure 15, ground motion is amplified through the soil column at VSAS.

All results from the EERA analyses are summarized in Tables 1 and 2. Input and output acceleration time histories are given in Appendix A. The input acceleration time histories at depth are shown, along with the actual free-field acceleration time histories and the theoretical EERA output time histories. The corresponding transfer functions from the EERA analysis are presented in Appendix B. As shown in Appendix B, the transfer functions at VSAP and VSAS are quite similar for different input motions and theoretically one transfer function should be used in the soil model.

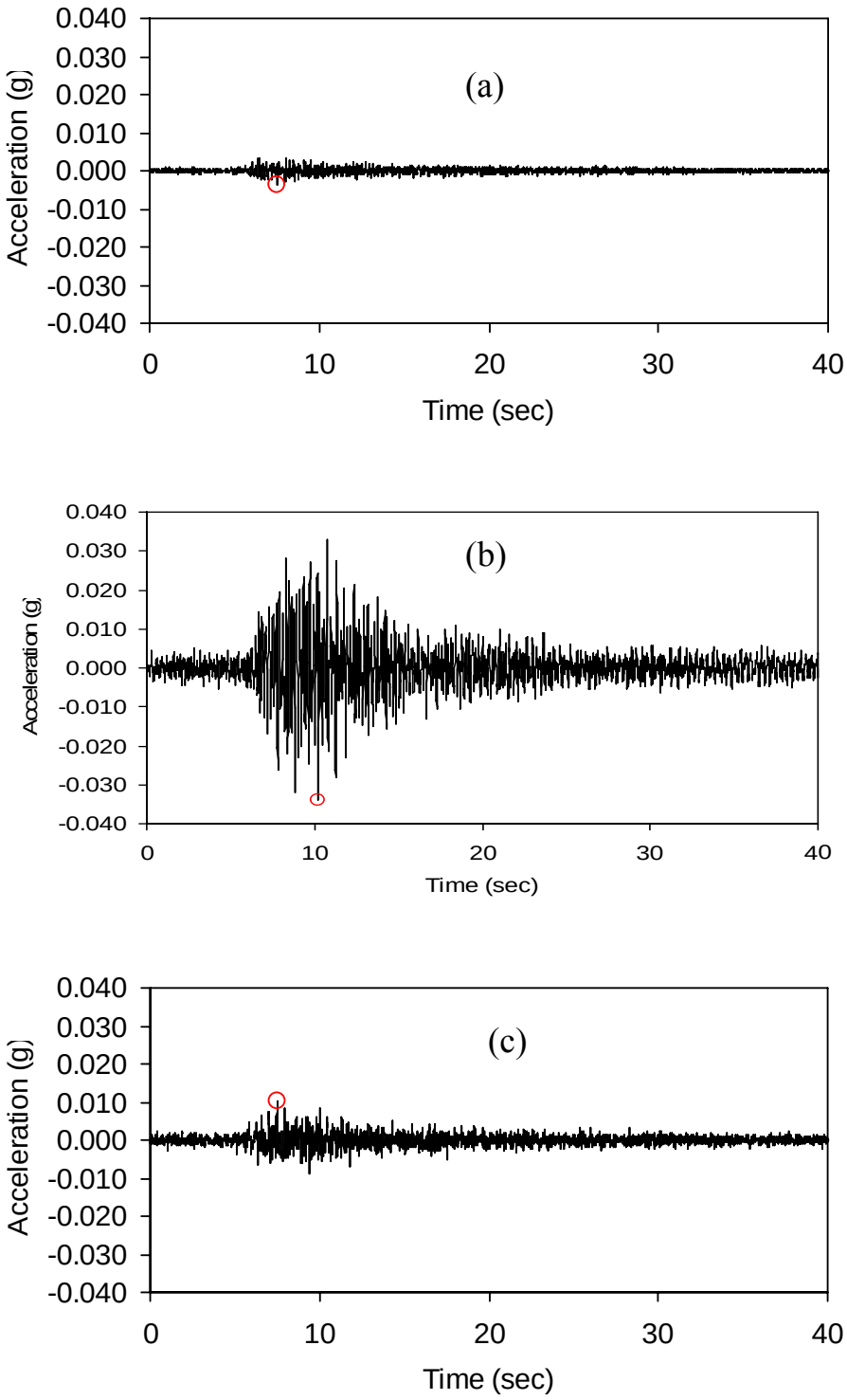

Figure 12. Input bedrock motion (recording from the April 18, 2008, southern Illinois earthquake) (a), output ground motion at free surface (b), and observed ground motion at free surface (c), at VSAP.

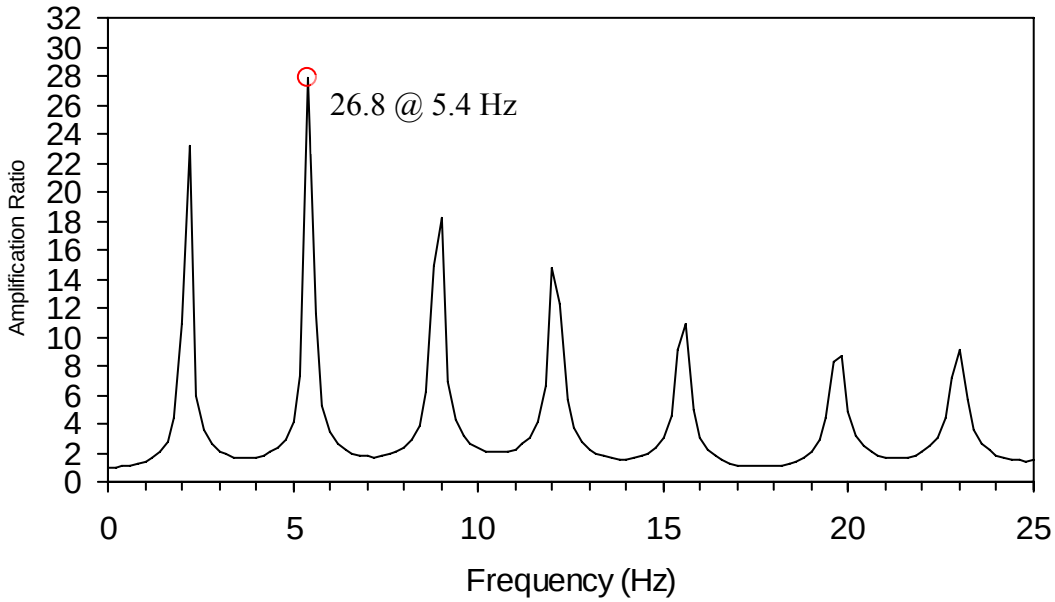

Figure 13. The transfer function at VSAP for the April 18, 2008, M5.2 southern Illinois earthquake.

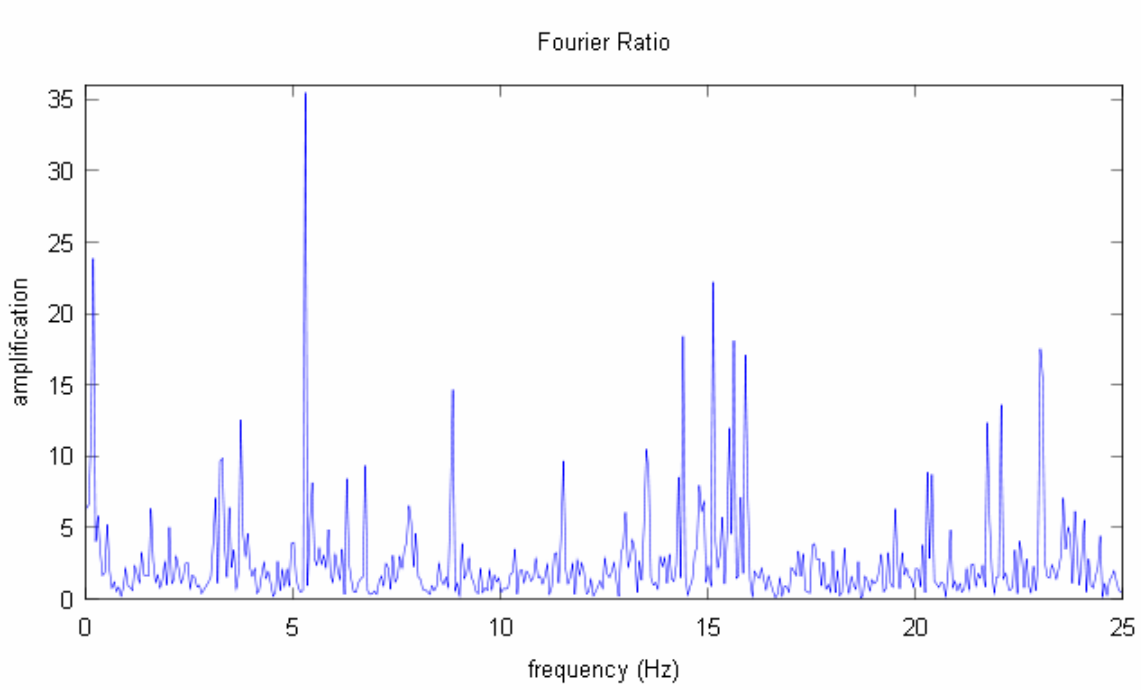

Figure 14. The spectral ratio between free-surface and bedrock recordings at VSAP from the April 18, 2008, southern Illinois earthquake.

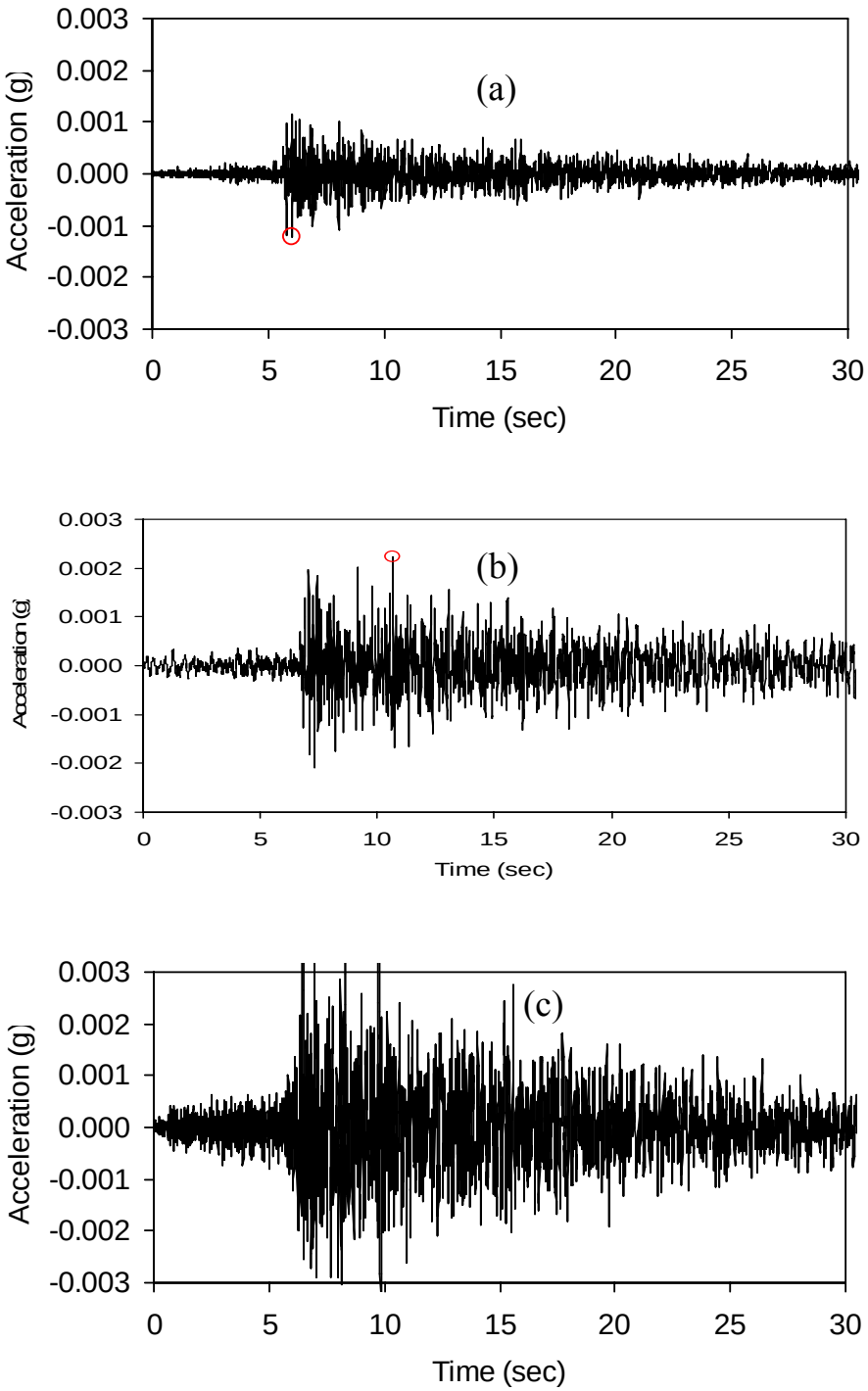

Figure 15. Input bedrock motion recording from the June 2, 2005, Ridgely, Tenn., earthquake (a), output ground motion at free surface (b), and observed ground motion at free surface (c), at VSAS.

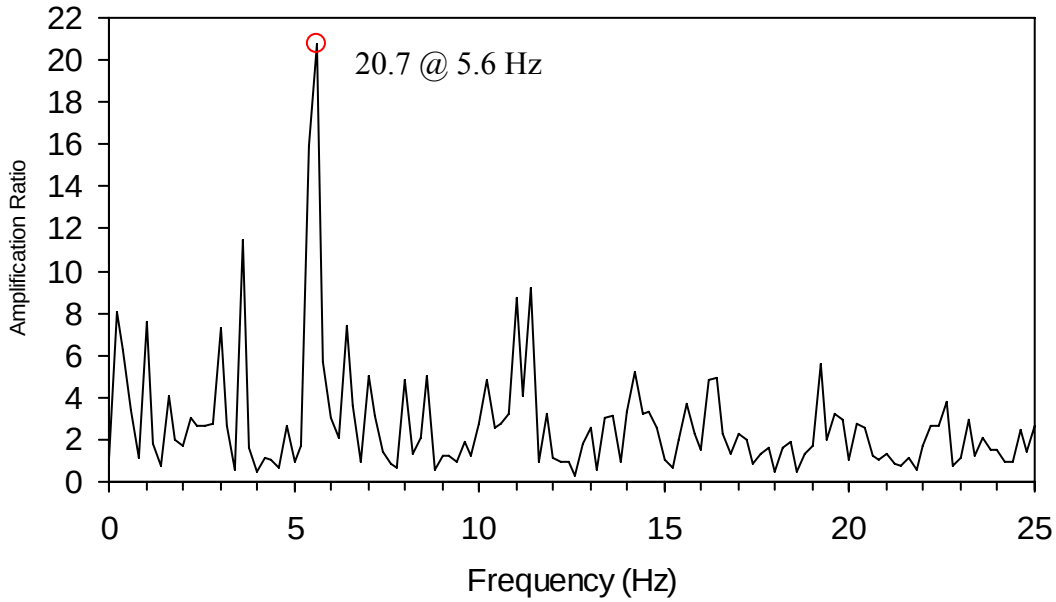

Figure 16. The transfer function at VSAS for the June 2, 2005, Ridgely, Tenn., earthquake.

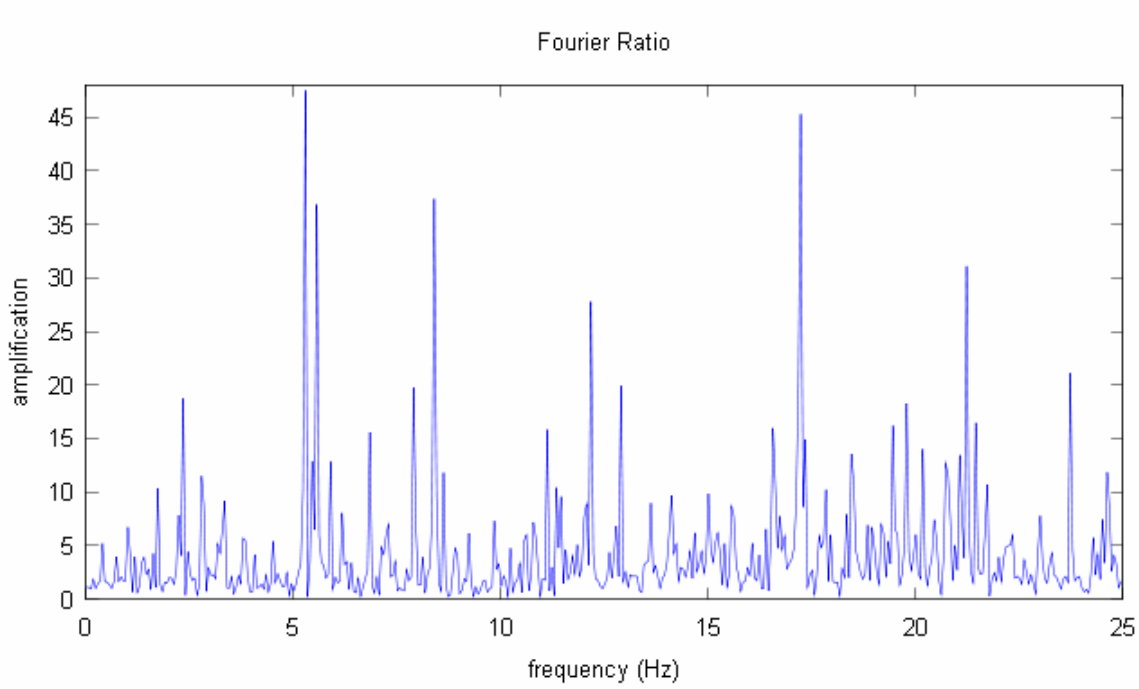

Figure 17. The spectral ratio between free-surface and bedrock recordings at VSAS from the June 2, 2005, Ridgely, Tenn., earthquake.

Table 1. Results of the equivalent linear analysis of seismic accelerations using EERA algorithms. Table of PGA values.

Earthquake	Lat. (N)	Long. (W)	Depth (km)	Distance from Sensors (km)	Accelerometer Orientation	PGA @ 100 m	PGA @ Surface	Theoretical PGA @ Surface
April 18, 2008 Southern Illinois M_w 5.2	38.45°	87.89°	11.6	168	transverse	0.0035 g	0.0102 g	0.0330 g
					longitudinal	0.0049 g	0.0135 g	0.0351 g
April 18, 2008 Southern Illinois M_w 4.6	38.48°	87.87°	10.0	171	transverse	0.0010 g	0.0026 g	0.0080 g
					longitudinal	0.0024 g	0.0062 g	0.0157 g
April 21, 2008 Southern Illinois M_w 4.0	38.49°	87.86°	10.0	173	transverse	0.0010 g	0.0024 g	0.0074 g
					longitudinal	0.0022 g	0.0044 g	0.0143 g
June 2, 2005 Ridgely, Tenn. M_w 3.9	36.15°	89.47°	15.1	124	transverse	0.0012 g	0.0015 g	0.0081 g
					longitudinal	0.0018 g	0.0026 g	0.0115 g
Earthquake	Lat. (N)	Long. (W)	Depth (km)	Distance from Sensors (km)	Accelerometer Orientation	PGA @ 260 m	PGA @ Surface	Theoretical PGA @ Surface
June 2, 2005 Ridgely, Tenn. M_w 3.9	36.15°	89.47°	15.1	46	transverse	0.0012 g	0.0046 g	0.0024 g
					longitudinal	0.0019 g	0.0045 g	0.0028 g
Feb. 10, 2005 Northeastern Arkansas M_w 4.1	35.76°	90.25°	15.5	121	transverse	0.0007 g	0.0028 g	0.0014 g
					longitudinal	0.0011 g	0.0028 g	0.0020 g
June 20, 2006 Blandville, Ky. M_w 3.6	36.92°	89.00°	8.9	50	transverse	0.0018 g	0.0046 g	0.0021 g
					longitudinal	0.0024 g	0.0065 g	0.0035 g

Table 2. Results of the equivalent linear analysis of seismic accelerations using EERA algorithms. Table of maximum amplification ratios and frequency.

Earthquake	Latitude (N)	Longitude (W)	Depth (km)	Epicentral Distance from sensors (km)	Accelerometer Orientation	Maximum Amplification Frequency (Hz)	Max. Ampl. Ratio
April 18, 2008 Southern Illinois M_w 5.2	38.45°	87.89°	11.6	168	transverse	5.4	26.8
					longitudinal	5.4	27.9
April 18, 2008 Southern Illinois M_w 4.6	38.48°	87.87°	10.0	171	transverse	5.4	26.8
					longitudinal	9.0	30.1
April 21, 2008 Southern Illinois M_w 4.0	38.49°	87.86°	10.0	173	transverse	9.0	28.9
					longitudinal	9.0	30.3
June 2, 2005 Ridgely, Tenn. M_w 3.9	36.15°	89.47°	15.1	124	transverse	9.0	28.9
					longitudinal	9.0	29.8
Earthquake	Latitude (N)	Longitude (W)	Depth (km)	Epicentral Distance from sensors (km)	Accelerometer Orientation	Maximum Amplification Frequency (Hz)	Max. Ampl. Ratio
June 2, 2005 Ridgely, Tenn. M_w 3.9	36.15°	89.47°	15.1	46	transverse	5.6	16.0
					longitudinal	5.6	20.7
Feb. 10, 2005 Northeastern Arkansas M_w 4.1	35.76°	90.25°	15.5	121	transverse	5.6	18.8
					longitudinal	5.6	20.4
June 20, 2006 Blandville, Ky. M_w 3.6	36.92°	89.00°	8.9	50	transverse	5.6	18.7
					longitudinal	5.6	20.6

CHAPTER FIVE

5. DISCUSSION

This study is unique for the central and eastern United States because it compares actual seismic ground motions at bedrock and the surface to theoretically derived synthetic ground motions. Detailed soil models were constructed from numerous geophysical and geotechnical methods, and an 1-D equivalent linear analysis of the soil response to earthquake ground motions utilizing the program EERA (Equivalent-linear Earthquake Response Analysis) was performed for six separate earthquakes. Acceleration time histories recorded at the soil-bedrock interface and at the surface (free-field) were used for the site response at VSAP. Acceleration time histories recorded at the surface (free-field) and at a depth of 260 m below ground surface were used for the site response at VSAS. The depth to bedrock at site VSAS is 590 m below ground surface; therefore, the time histories for the 260-m-deep accelerometer were filtered by the soil between the bedrock surface and the accelerometer. A project is under way to install seismic instruments within the bedrock at the VSAS site, thus minimizing this source of uncertainty.

For site VSAP, the dominant site frequency is about 5.4 Hz with a spectral ratio of about 30. The observations show a spectral ratio of about 35 at the dominant frequency of about 6 Hz. In terms of peak ground acceleration, the EERA model overpredicts free-field PGA at site VSAP two to three times, in comparison with the actual recorded free-field accelerations.

For site VSAS, the dominant site frequency is about 5.6 Hz with a spectral ratio of about 20. The observations show a spectral ratio of about 45 at the dominant frequency

of about 6 Hz. In terms of peak ground acceleration, the EERA model underpredicts free-field PGA at site VSAS about two times, in comparison with the actual recorded free-field accelerations.

This study indicates that procedures used to evaluate the site response of deep soil sites do capture most of the site amplification feature. It also suggests that the procedures need to be evaluated with as much detail as possible in order to produce an accurate representation of the actual ground-motion response.

There are a variety of reasons for the discrepancy between the actual and theoretical PGA and frequency of the ground motions. The soil model may be inaccurate or not detailed enough, or a variety of three-dimensional effects may influence the recorded ground motions. The recording instruments are located near the edge of the Upper Mississippi embayment; however, the EERA model is based on flat layers in two dimensions. The added geometrical variation in the real-world model is not accounted for in the EERA model. Both scattering and concentration of the seismic energy can occur. In addition, waves resonating within the soil column due to the geometry of the basin could and will influence how the EERA-model ground motions compare to the actual ground motions at the site.

CHAPTER SIX

6. CONCLUSIONS

Six earthquake acceleration time histories were used to evaluate the ground-motion response of two sites, VSAP and VSAS, near the New Madrid Seismic Zone. These earthquakes ranged in magnitude from M_w 3.6 to M_w 5.2 and were located 46 to 173 km away from the recording instruments. These two sites are underlain by thick sequences (100 and 590 m) of unlithified soil that have been shown to greatly influence earthquake ground motions.

The generalized soil models were used for the EERA analysis at sites VSAP and VSAS. The results indicate that procedures used to evaluate the site response of deep soil sites do capture most of the site amplification feature. The results also suggest that the procedures need to be evaluated with as much detail as possible in order to produce an accurate representation of the actual ground-motion response. This study also shows that more detailed analysis (e.g., 3-D) of how deep soil sites respond to ground shaking are needed to help engineers and scientists understand the ground-motion amplification in the central United States.

APPENDIX A

Acceleration Time Histories

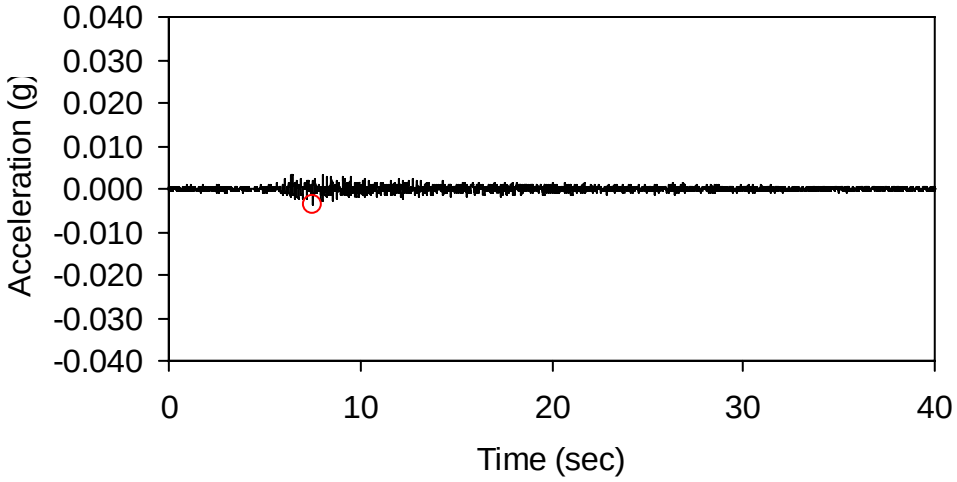

Figure A-1.VSAP M5.2 Southern Illinois transverse sensor (100 m) actual (0.0035 g)

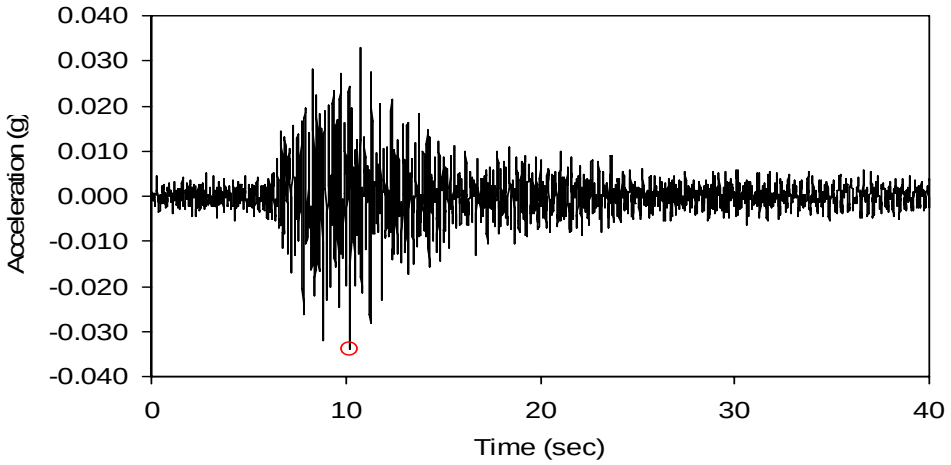

Figure A-2. VSAP M5.2 Southern Illinois transverse sensor (free-field) theoretical (0.0330 g)

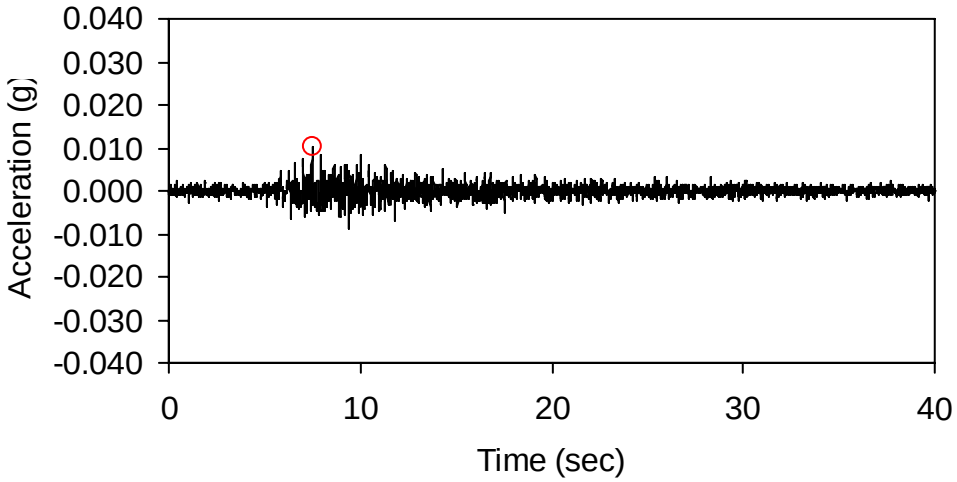

Figure A-3. VSAP M5.2 Southern Illinois transverse sensor (free-field) actual (0.0102 g)

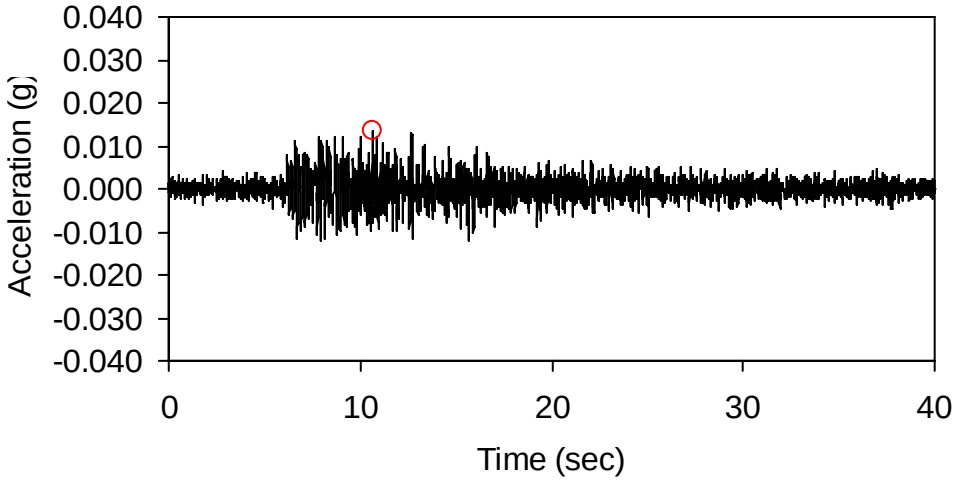

Figure A-4. VSAP M5.2 Southern Illinois longitudinal sensor (100 m) actual (0.0049 g)

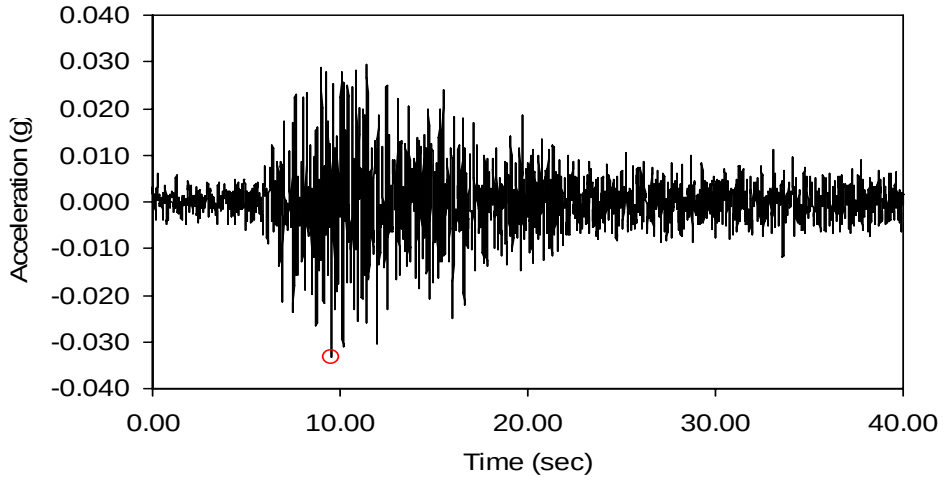

Figure A-5. VSAP M5.2 Southern Illinois longitudinal sensor (free-field) theoretical (0.0351 g)

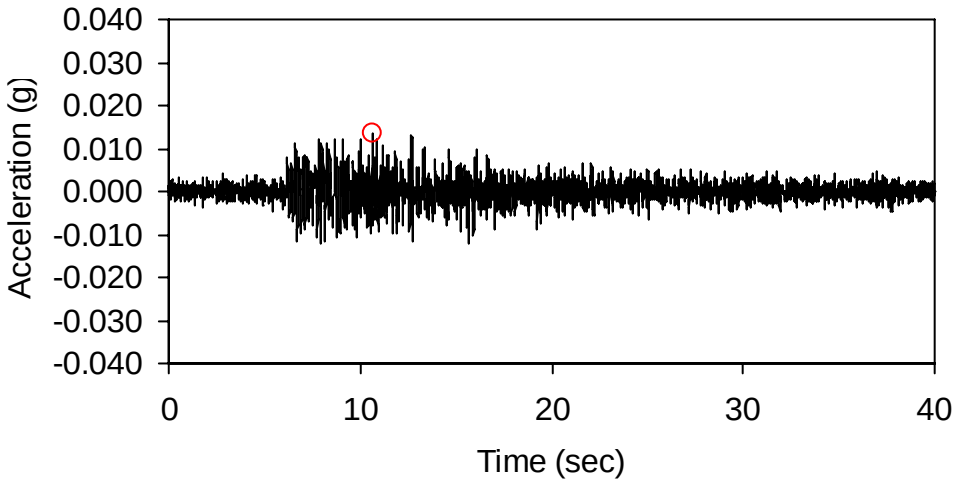

Figure A-6. VSAP M5.2 Southern Illinois longitudinal sensor (free-field) actual (0.0135 g)

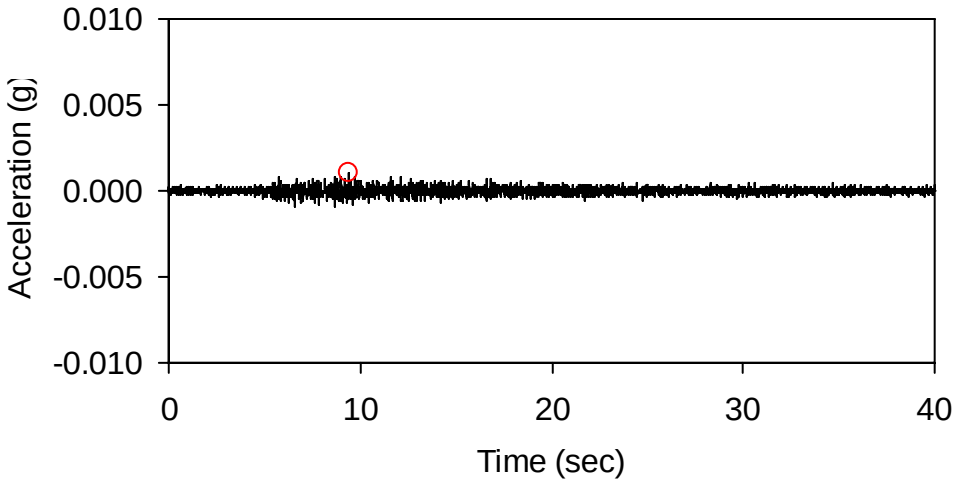

Figure A-7. VSAP M4.6 Southern Illinois transverse sensor (100 m) actual (0.0010 g)

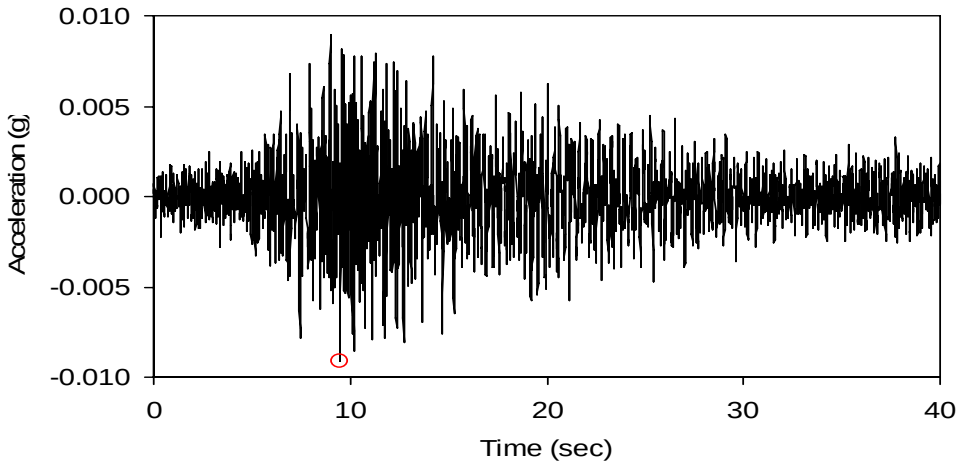

Figure A-8. VSAP M4.6 Southern Illinois transverse sensor (free-field) theoretical (0.0080 g)

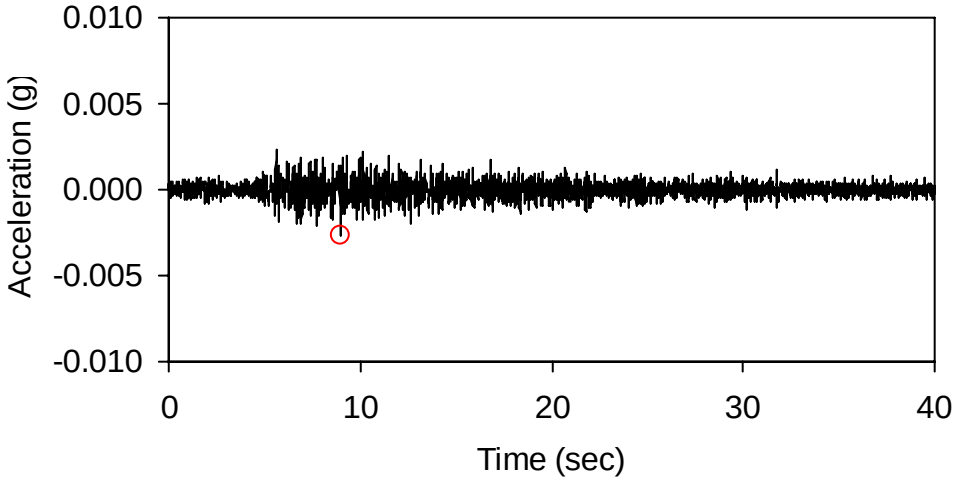

Figure A-94. VSAP M4.6 Southern Illinois transverse sensor (free-field) actual (0.0026 g)

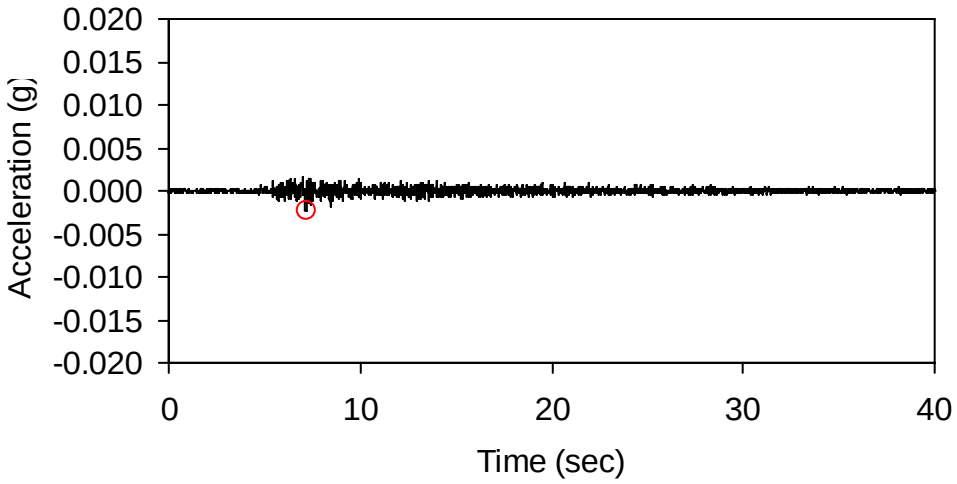

Figure A-10. VSAP M4.6 Southern Illinois longitudinal sensor (100 m) actual (0.0024 g)

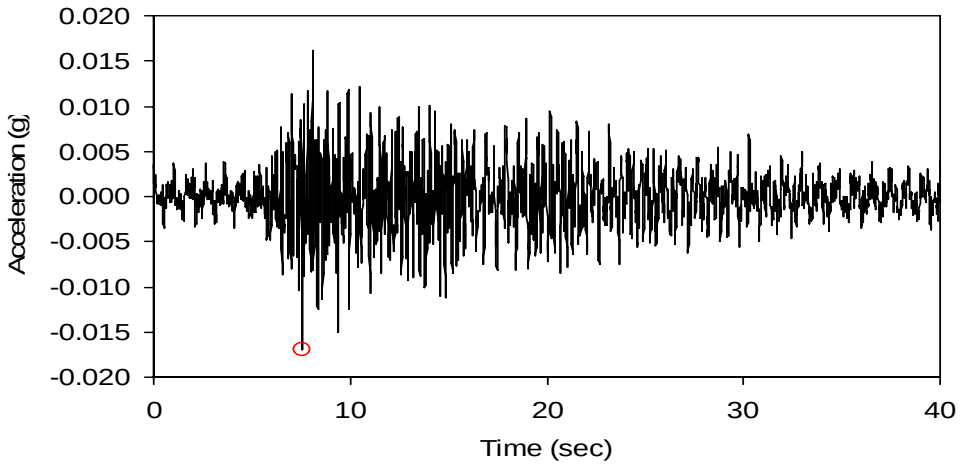

Figure A-51. VSAP M4.6 Southern Illinois longitudinal sensor (free-field) theoretical (0.0157 g)

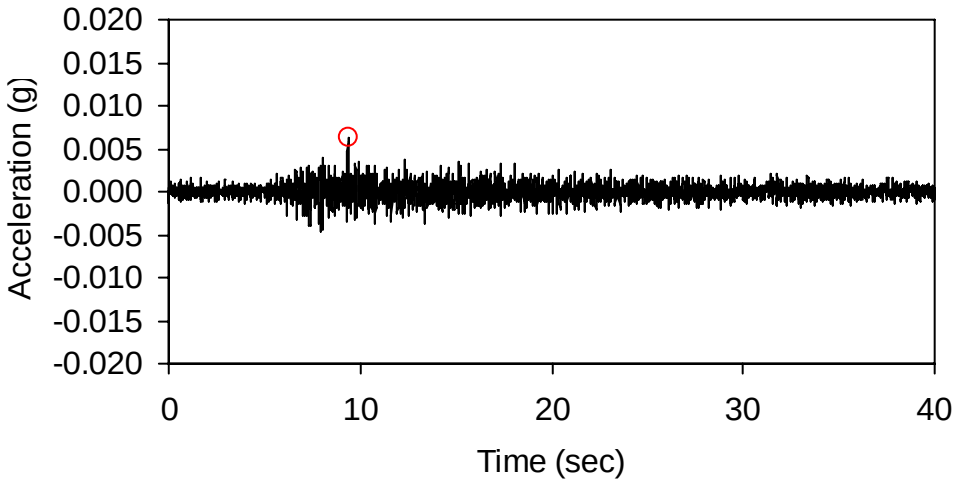

Figure A-62. VSAP M4.6 Southern Illinois longitudinal sensor (free-field) actual (0.0062 g)

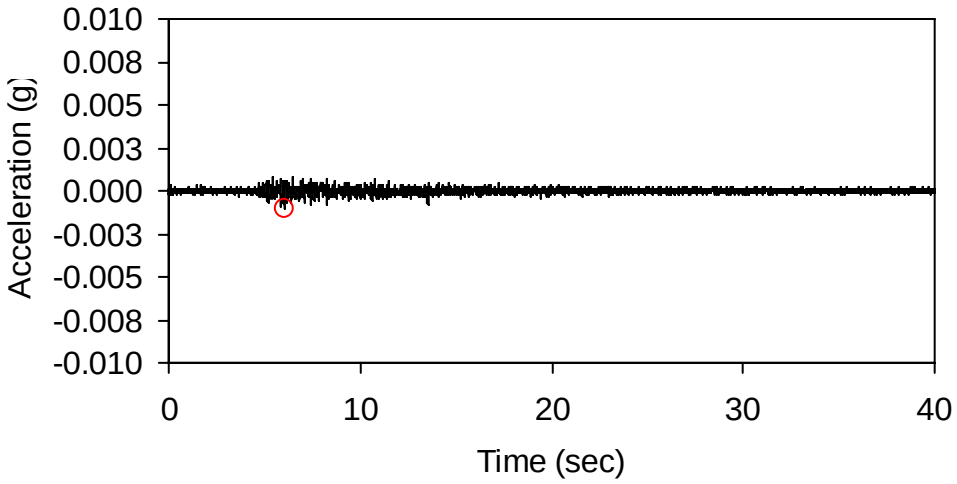

Figure A-73. VSAP M4.0 Southern Illinois transverse sensor (100 m) actual (0.0010 g)

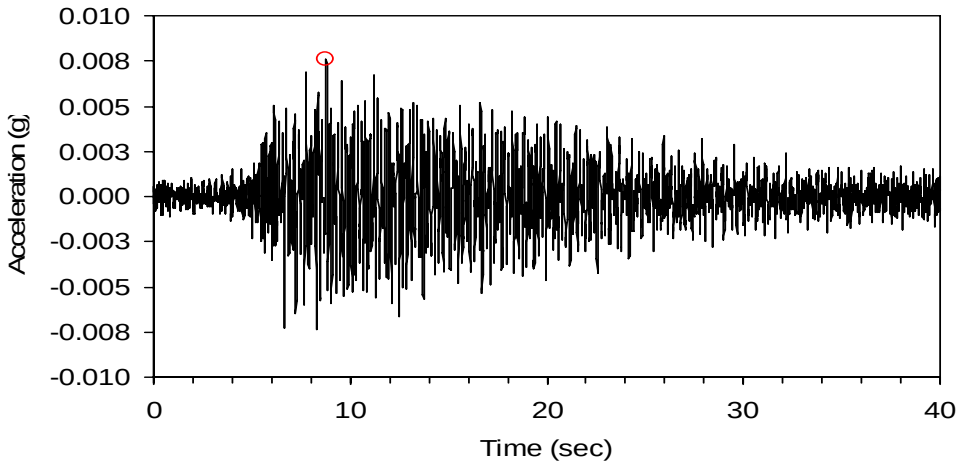

Figure A-14. VSAP M4.0 Southern Illinois transverse sensor (free-field) theoretical (0.0074 g)

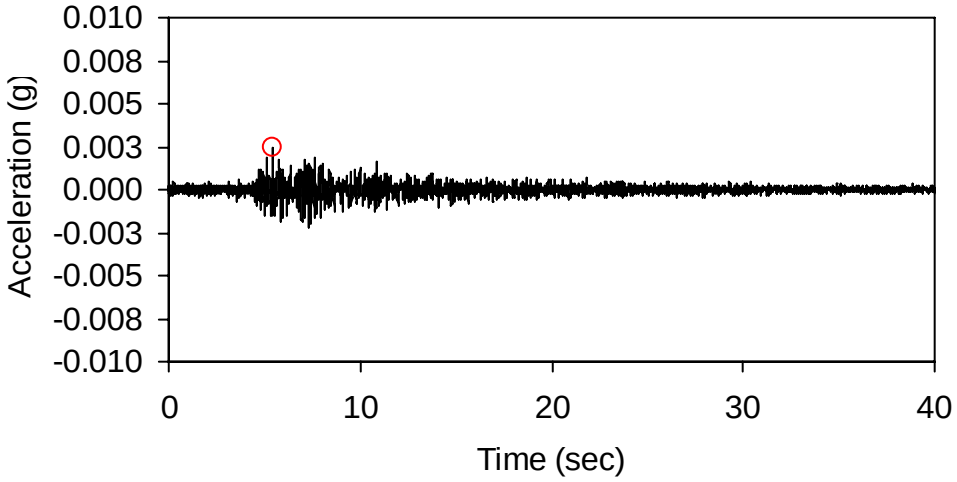

Figure A-15. VSAP M4.0 Southern Illinois transverse sensor (free-field) actual (0.0024 g)

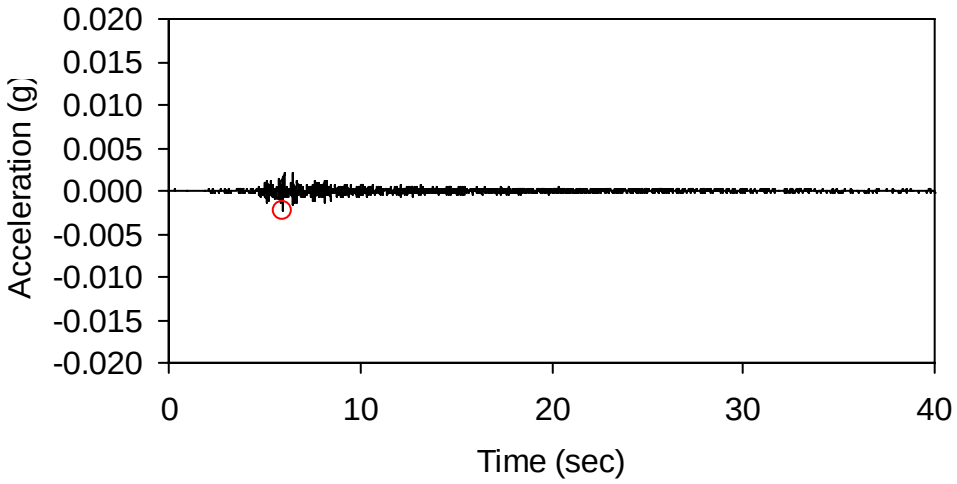

Figure A-16. VSAP M4.0 Southern Illinois longitudinal sensor (100 m) actual (0.0022 g)

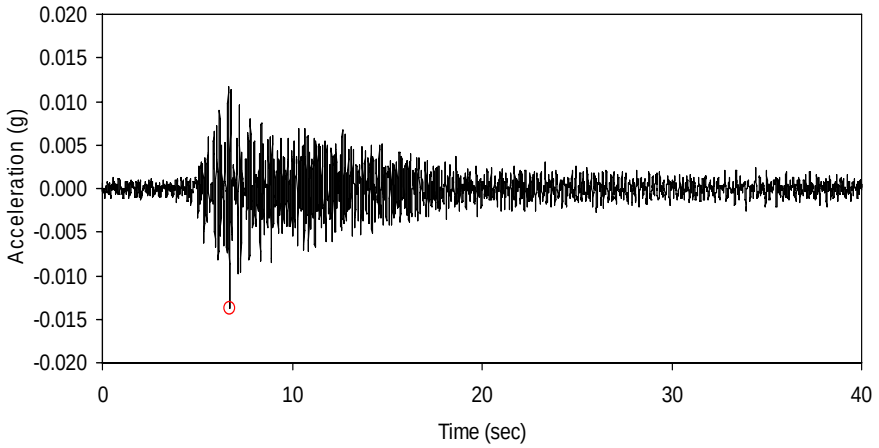

Figure A-17. VSAP M4.0 Southern Illinois longitudinal sensor (free-field) theoretical (0.0143 g)

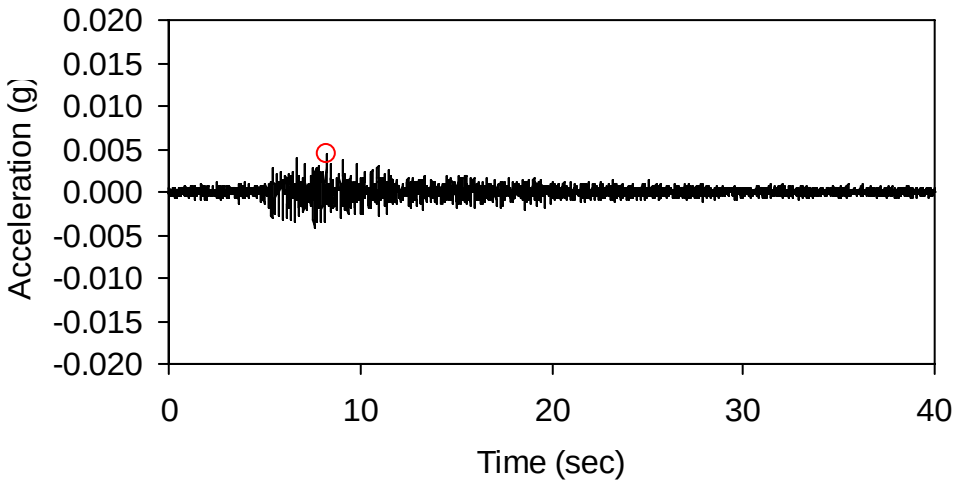

Figure A-18. VSAP M4.0 Southern Illinois longitudinal sensor (free-field) actual (0.0044 g)

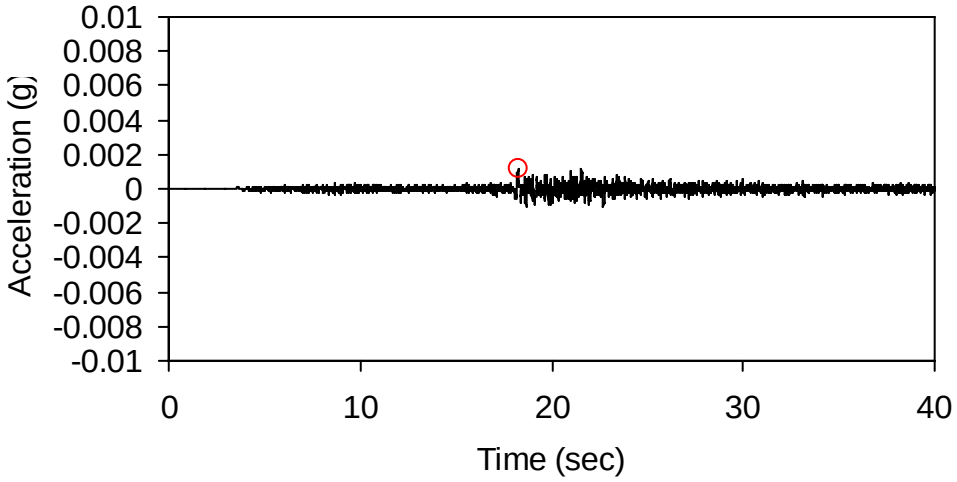

Figure A-19. VSAP M3.9 Ridgely, Tenn. transverse sensor (100 m) actual (0.0012 g)

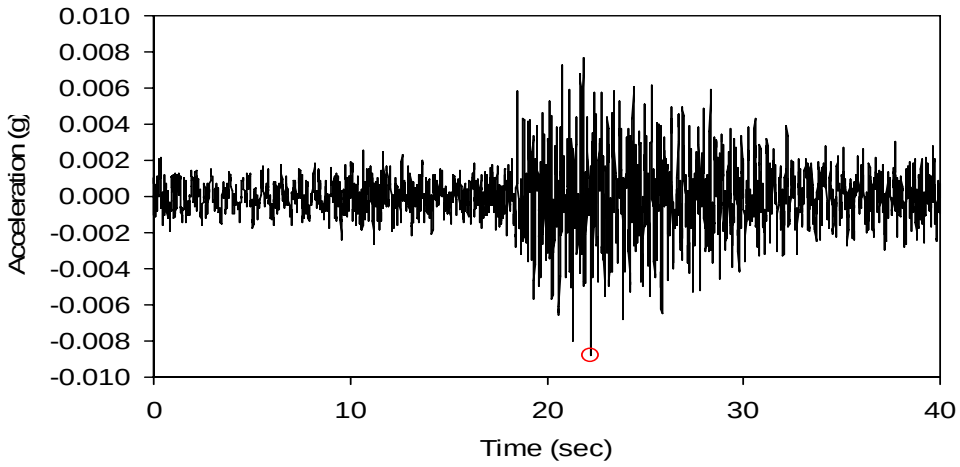

Figure A-20. VSAP M3.9 Ridgely, Tenn. transverse sensor (free-field) theoretical (0.0081 g)

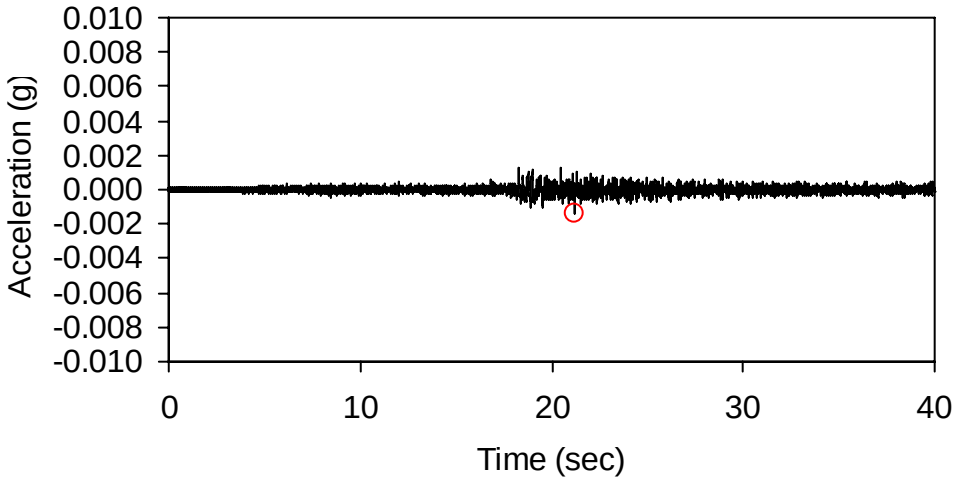

Figure A-21. VSAP M3.9 Ridgely, Tenn. transverse sensor (free-field) actual (0.0015 g)

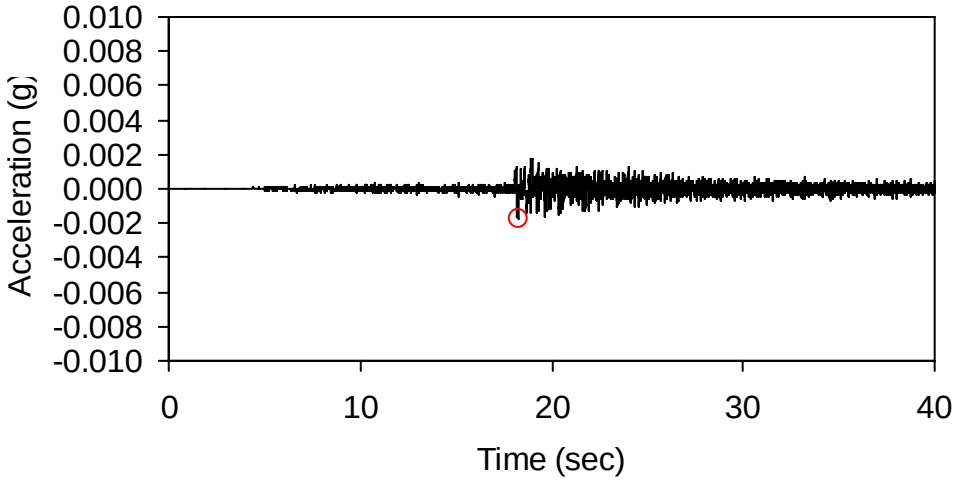

Figure A-22. VSAP M3.9 Ridgely, Tenn. longitudinal sensor (100 m) actual (0.0018 g)

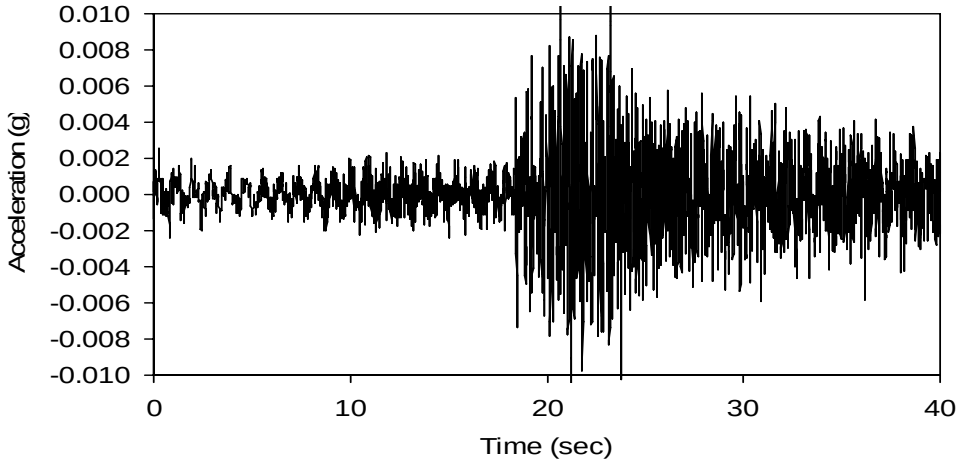

Figure A-23. VSAP M3.9 Ridgely, Tenn. longitudinal sensor (free-field) theoretical (0.0115 g)

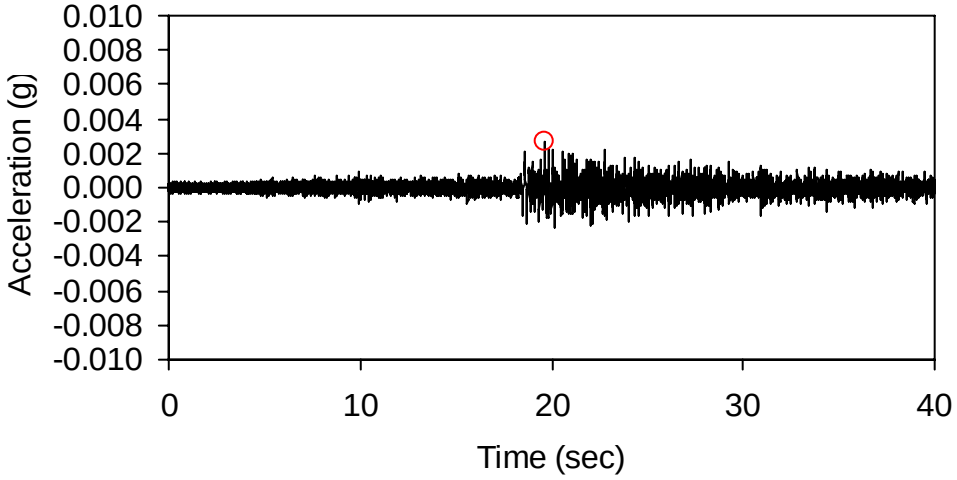

Figure A-24. VSAP M3.9 Ridgely, Tenn. longitudinal sensor (free-field) theoretical (0.0026 g)

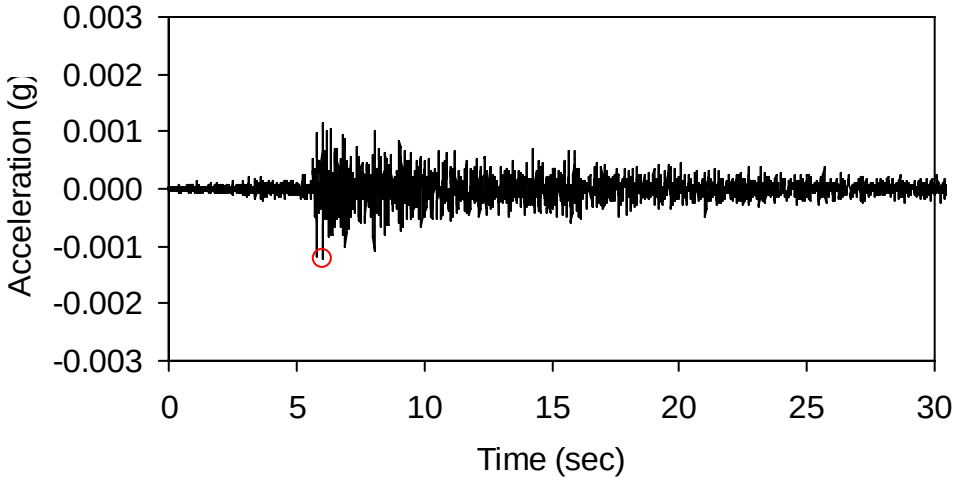

Figure A-25. VSAS M3.9 Ridgely, Tenn. transverse sensor (260 m) actual (0.0012 g)

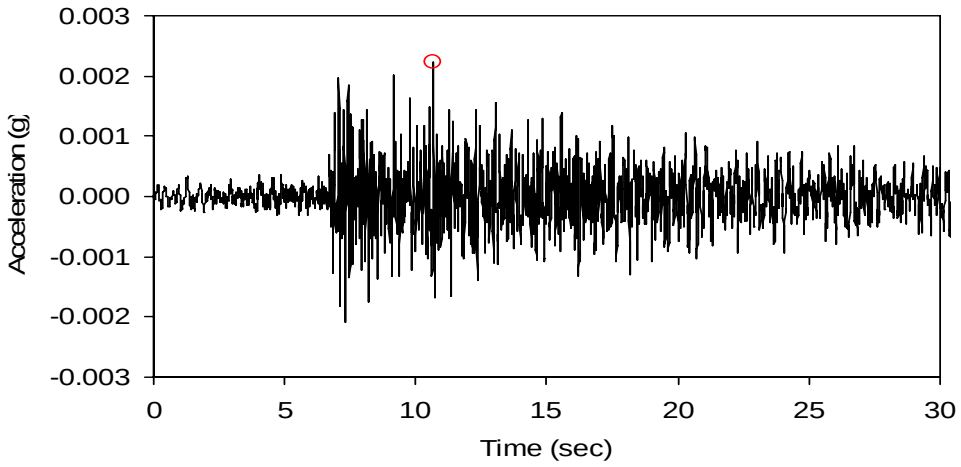

Figure A-26. VSAS M3.9 Ridgely, Tenn. transverse (free-field) theoretical (0.0024 g)

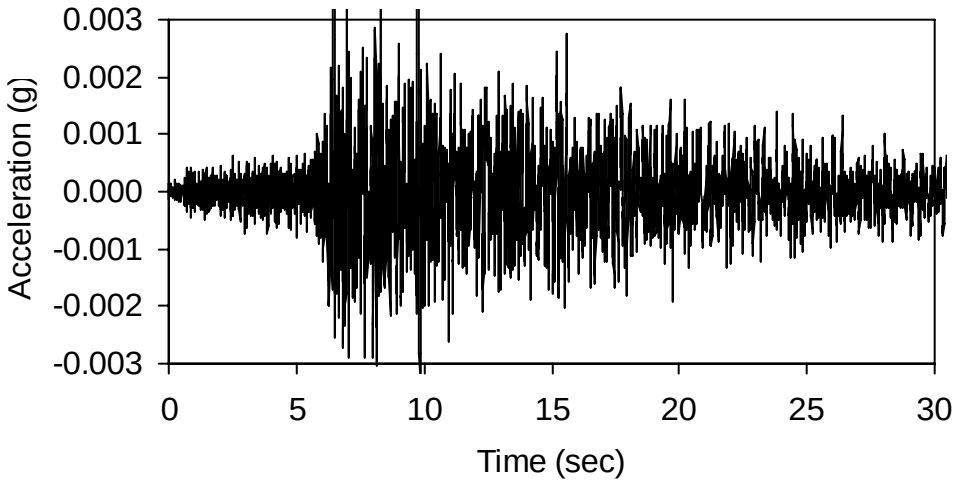

Figure A-27. VSAS M3.9 Ridgely, Tenn. transverse sensor (free-field) actual (0.0046 g)

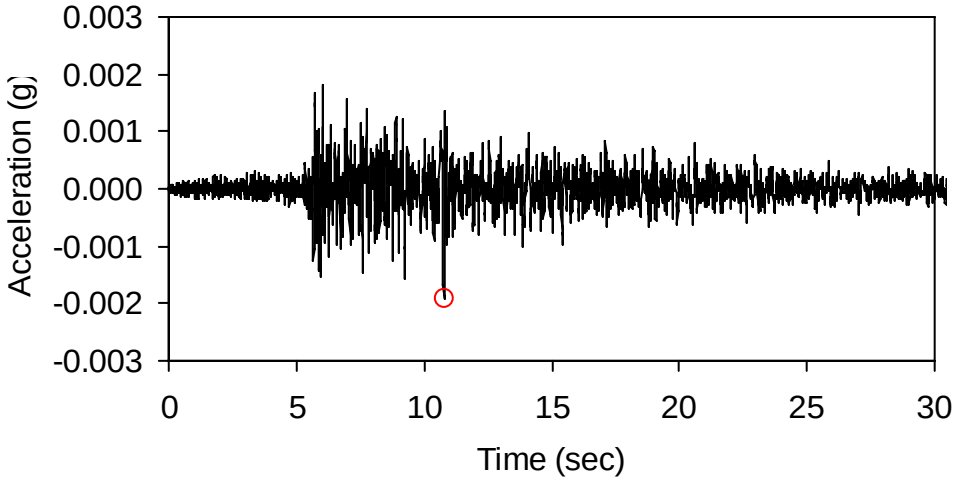

Figure A-28. VSAS M3.9 Ridgely, Tenn. longitudinal sensor (260 m) actual (0.0019 g)

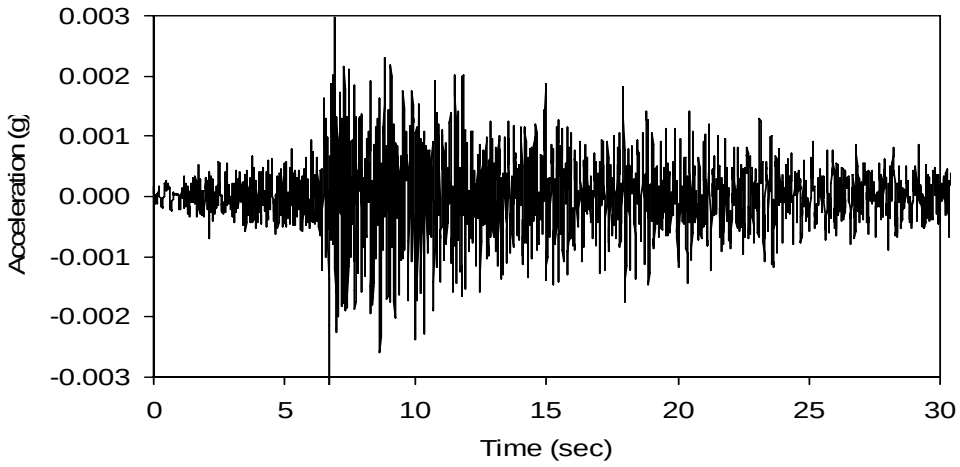

Figure A-29. VSAS M3.9 Ridgely, Tenn. longitudinal sensor (free-field) theoretical (0.0028 g)

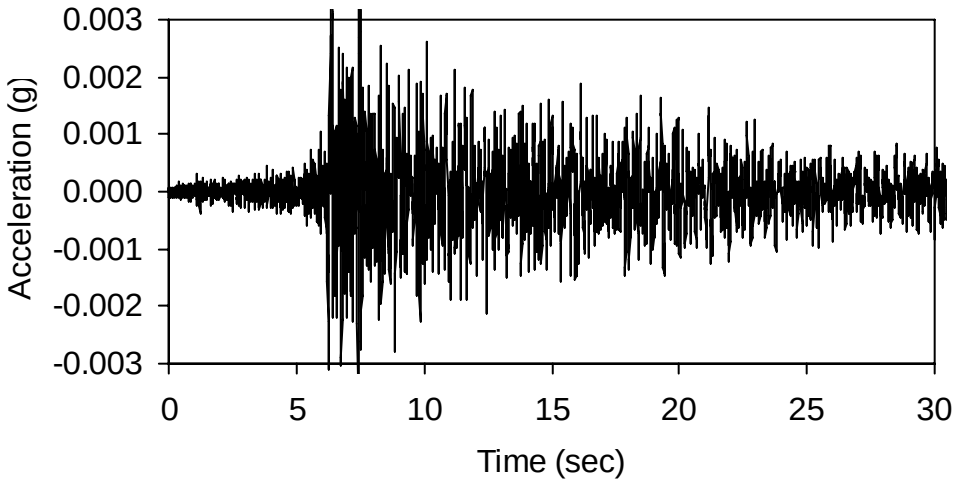

Figure A-30. VSAS M3.9 Ridgely, Tenn. longitudinal sensor (free-field) actual (0.0045 g)

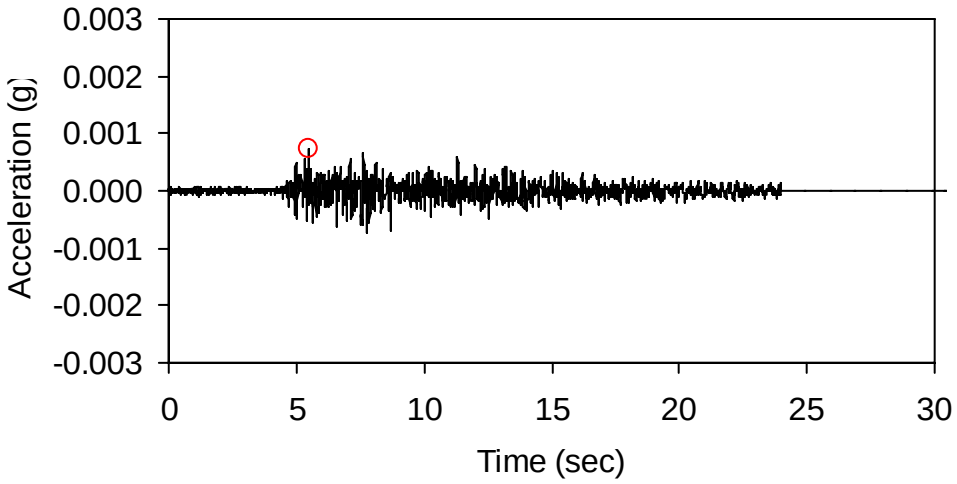

Figure A-31. VSAS M4.1 Arkansas transverse sensor (260 m) actual (0.0007 g)

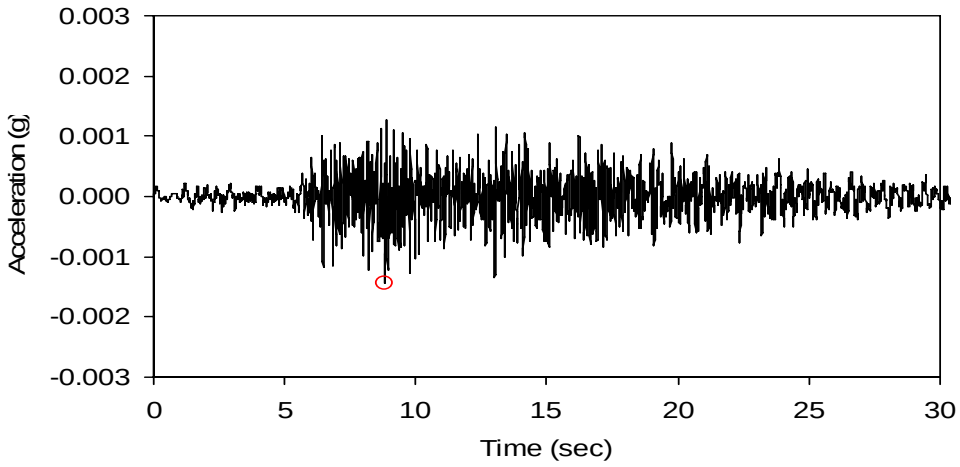

Figure A-32. VSAS M4.1 Arkansas transverse sensor (free-field) theoretical (0.0014 g)

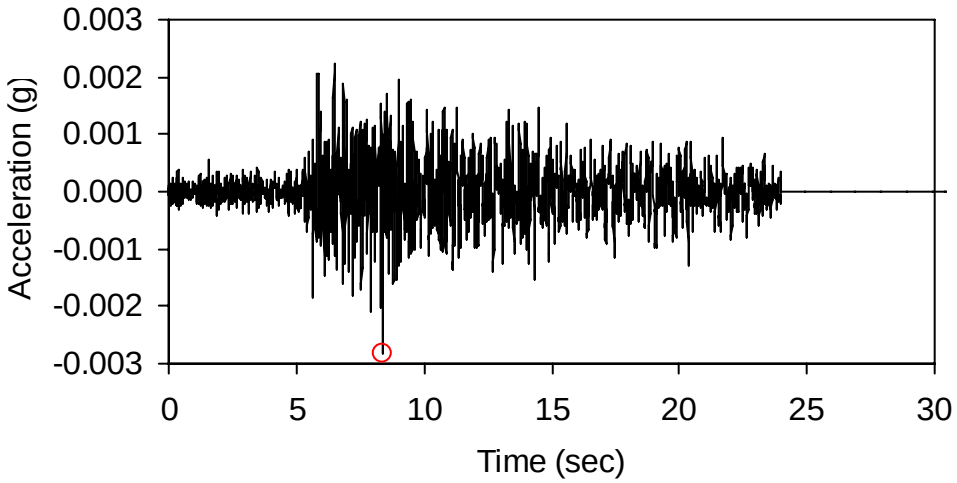

Figure A-33. VSAS M4.1 Arkansas transverse sensor (free-field) actual (0.0028 g)

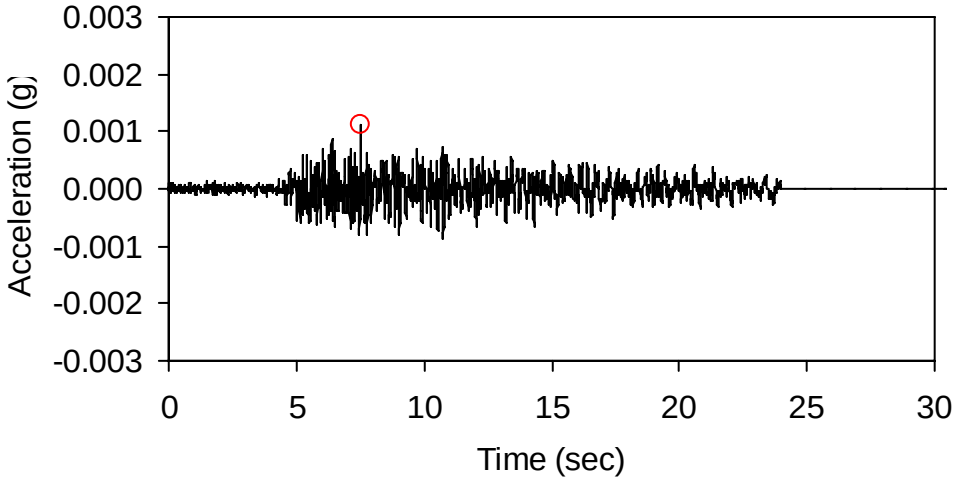

Figure A-34. VSAS M4.1 Arkansas longitudinal sensor (260 m) actual (0.0011 g)

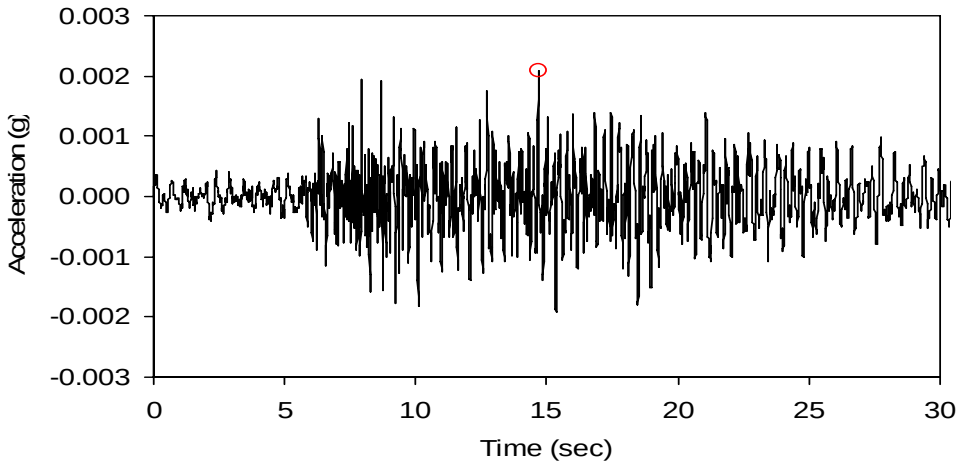

Figure A-35. VSAS M4.1 Arkansas longitudinal sensor (free-field) theoretical (0.0020 g)

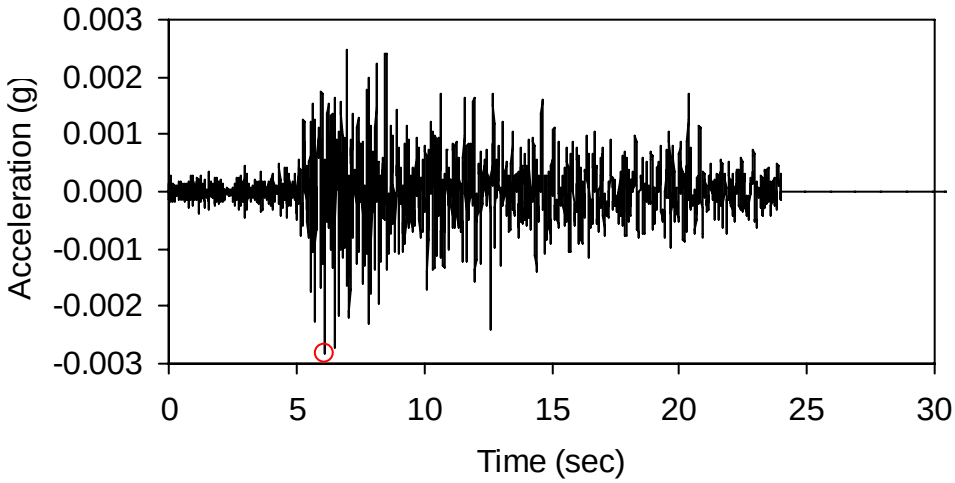

Figure A-36. VSAS M4.1 Arkansas longitudinal sensor (free-field) actual (0.0028 g)

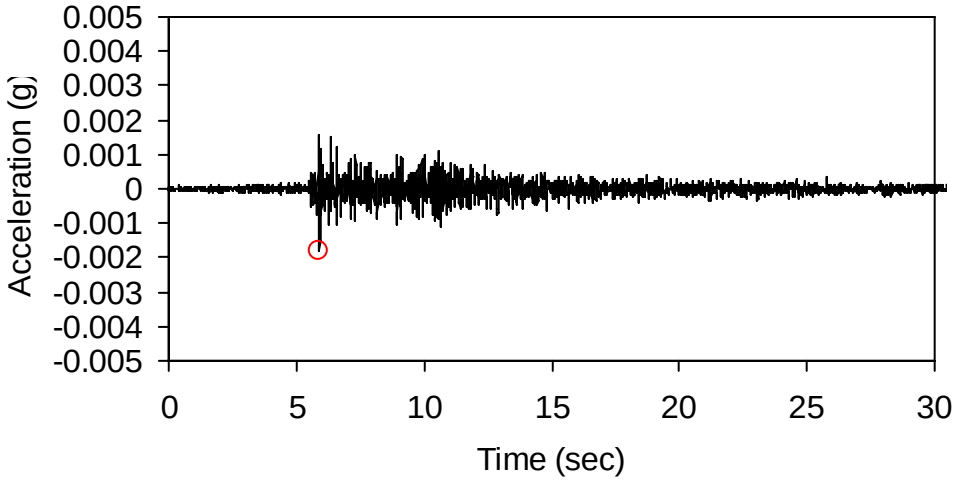

Figure A-37. VSAS M3.6 Blandville, Ky. transverse sensor (260 m) actual (0.0018 g)

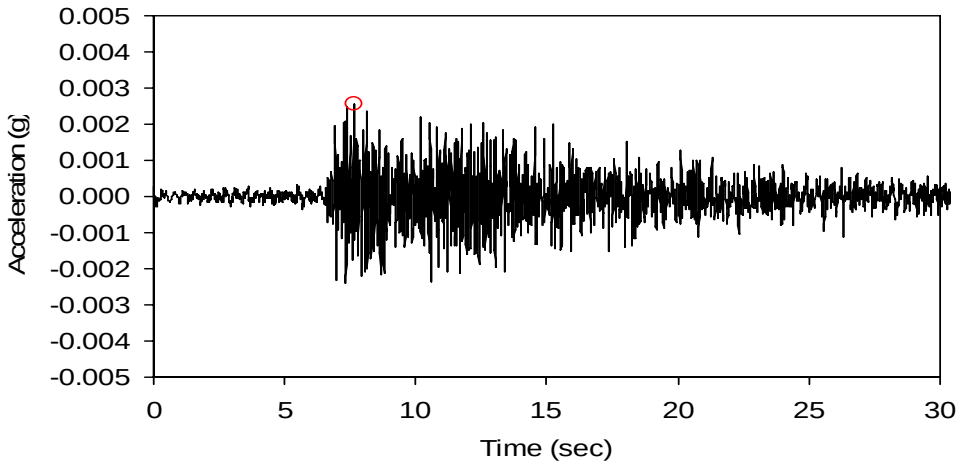

Figure A-38. VSAS M3.6 Blandville, Ky. transverse sensor (free-field) theoretical (0.0021 g)

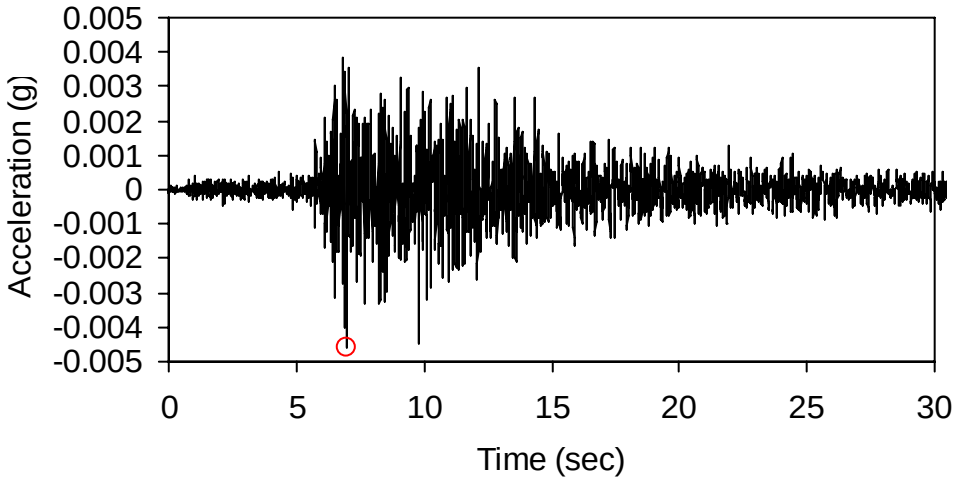

Figure A-39. VSAS M3.6 Blandville, Ky. transverse sensor (free-field) actual (0.0046 g)

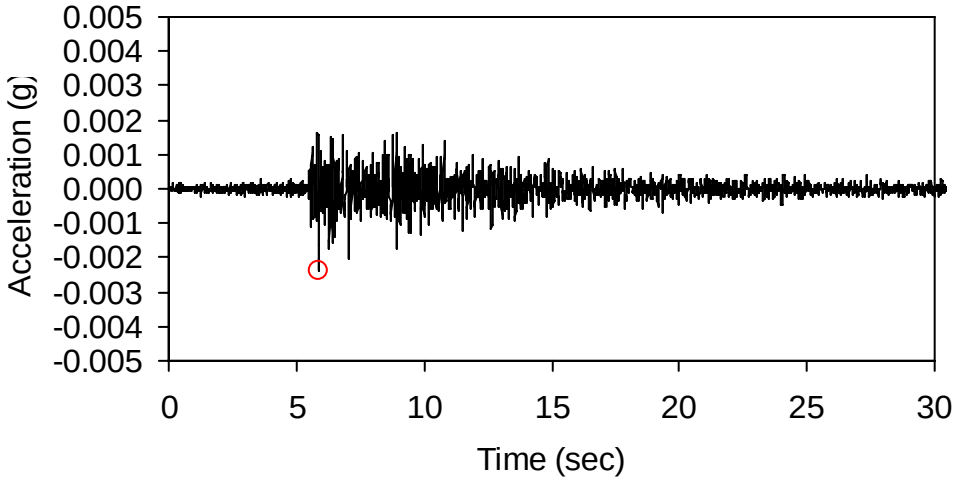

Figure A-40. VSAS M3.6 Blandville, Ky. longitudinal sensor (260 m) actual (0.0024 g)

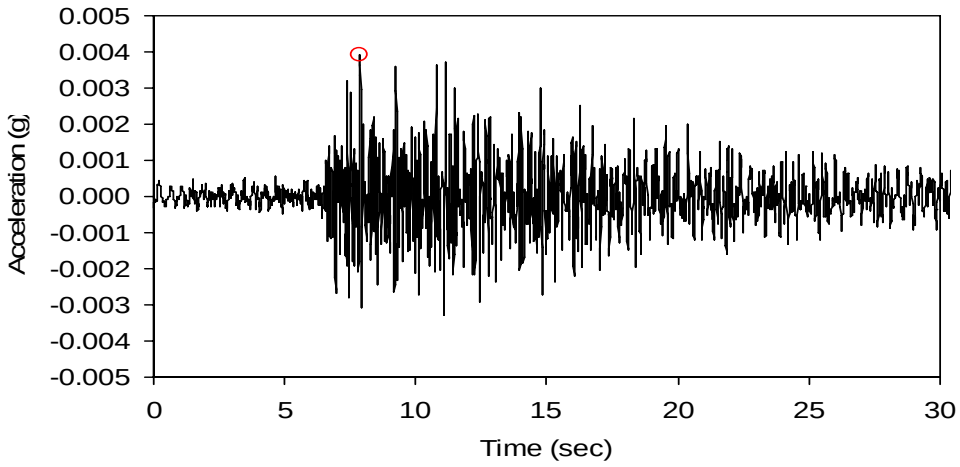

Figure A-41. VSAS M3.6 Blandville, Ky. longitudinal sensor (free-field) theoretical (0.0035 g)

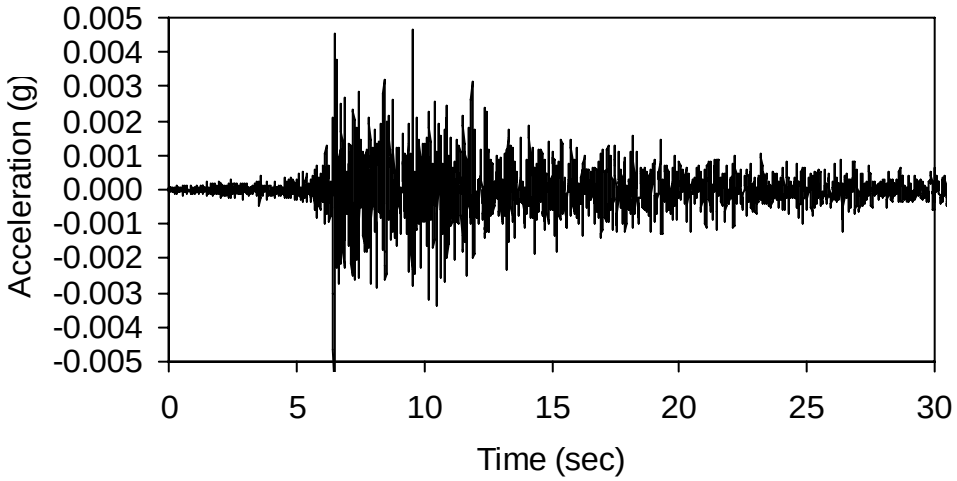

Figure A-42. VSAS M3.6 Blandville, Ky. longitudinal sensor (free-field) actual (0.0065 g)

APPENDIX B

Transfer Functions/Amplification Ratios

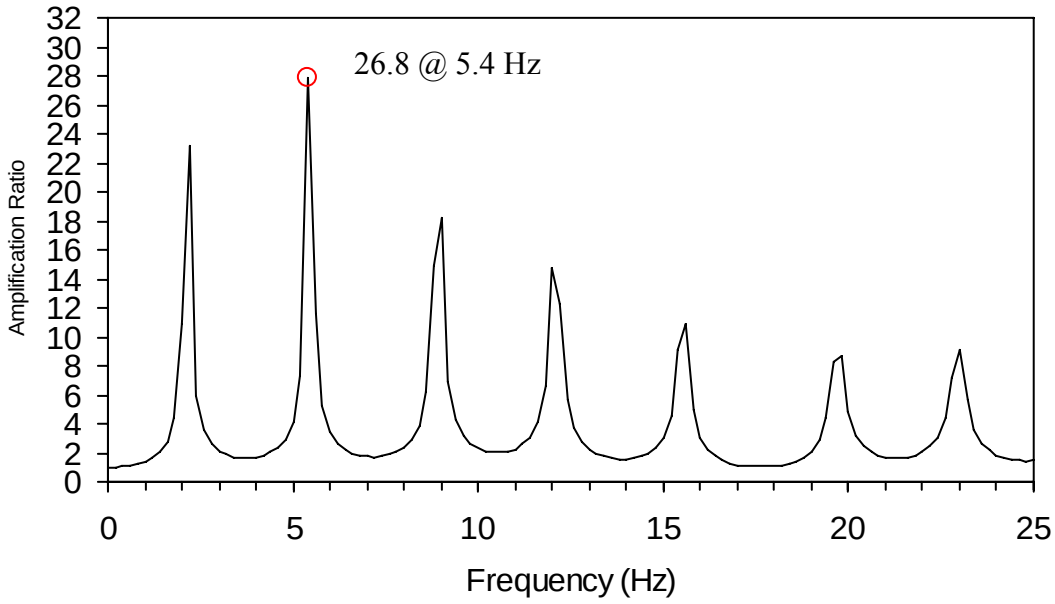

Figure B-1. VSAP M5.2 Southern Illinois transverse sensor transfer function.

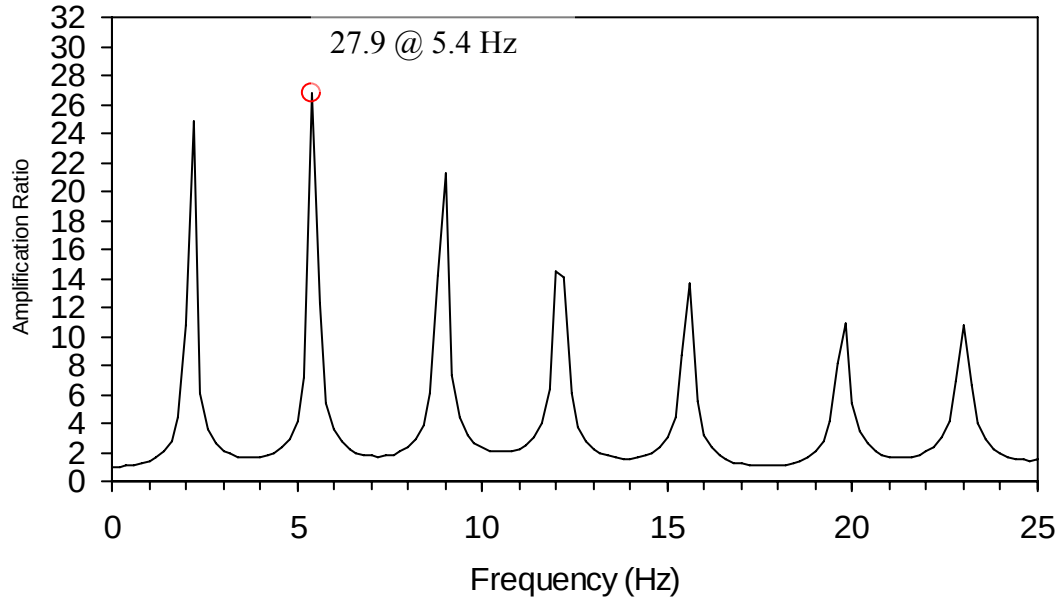

Figure B-2. VSAP M5.2 Southern Illinois longitudinal sensor transfer function.

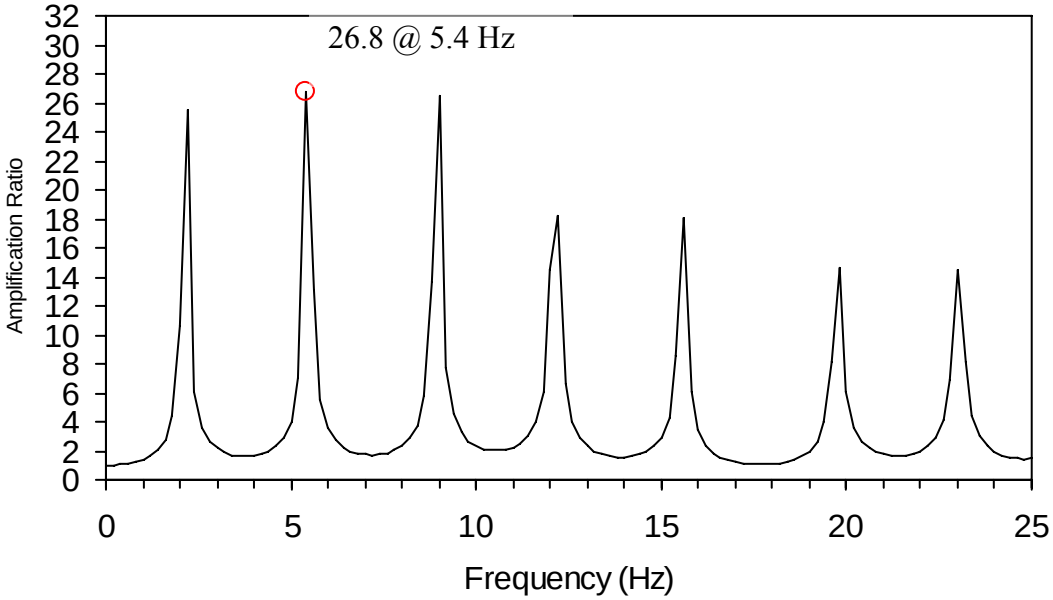

Figure B-3. VSAP M4.6 Southern Illinois transverse sensor transfer function.

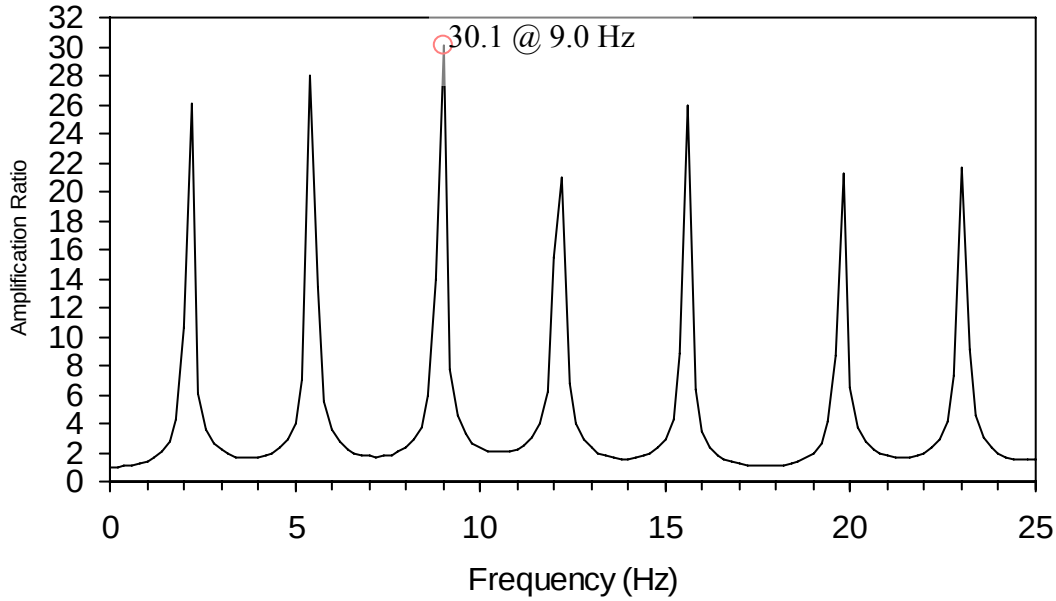

Figure B-4. VSAP M4.6 Southern Illinois longitudinal sensor transfer function.

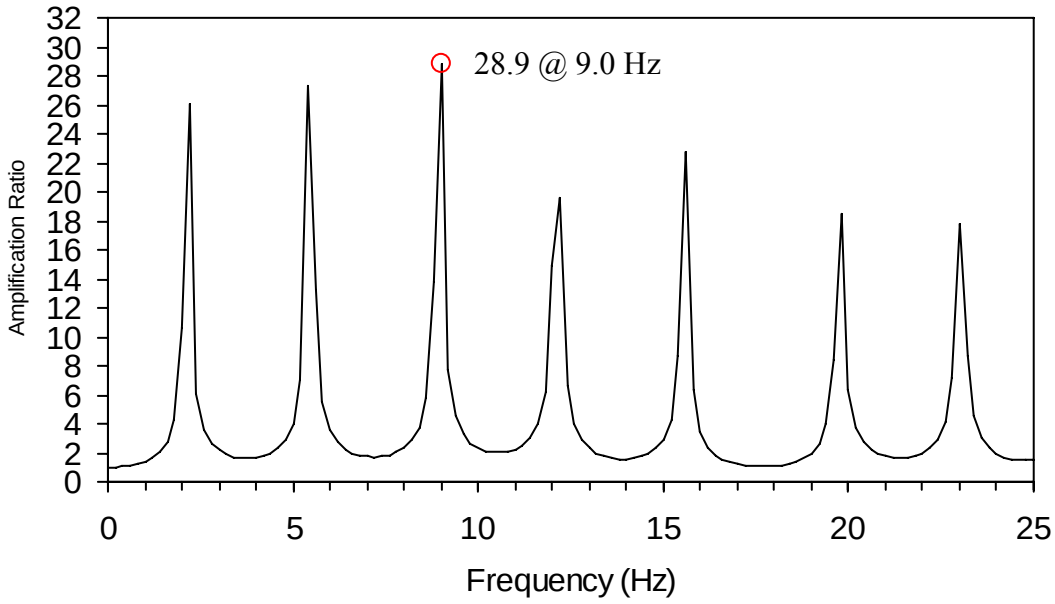

Figure B-5. VSAP M4.0 Southern Illinois transverse sensor transfer function.

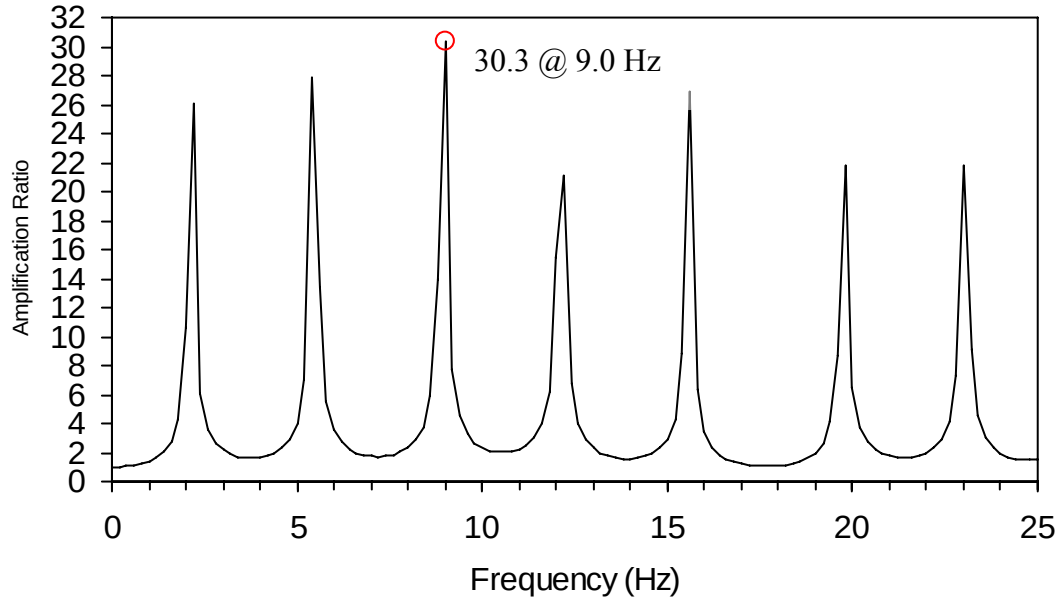

Figure B-6. VSAP M4.0 Southern Illinois longitudinal sensor transfer function.

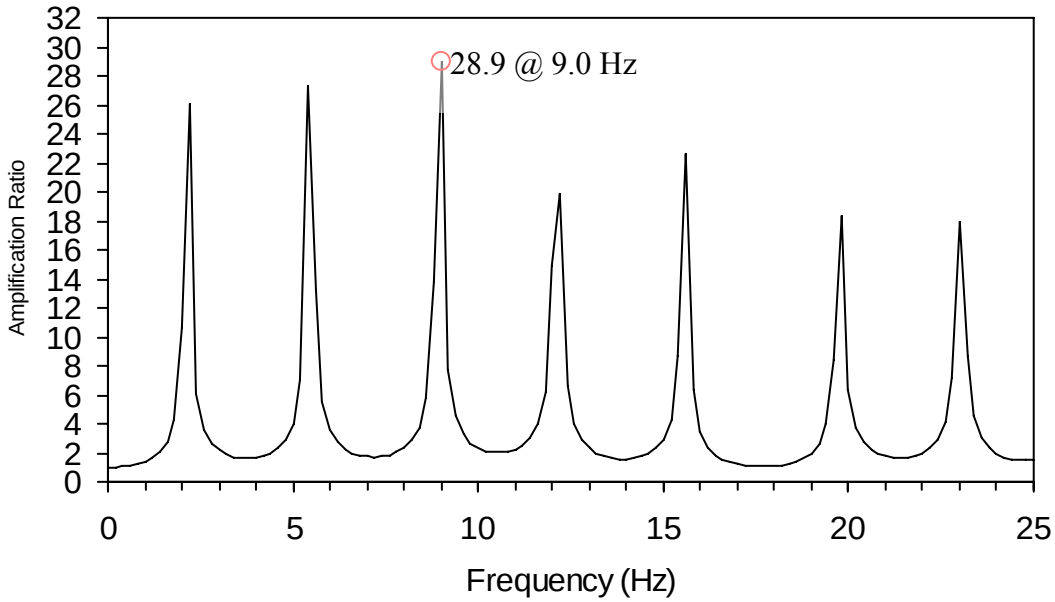

Figure B-7. VSAP M3.9 Ridgely, Tenn. transverse sensor transfer function.

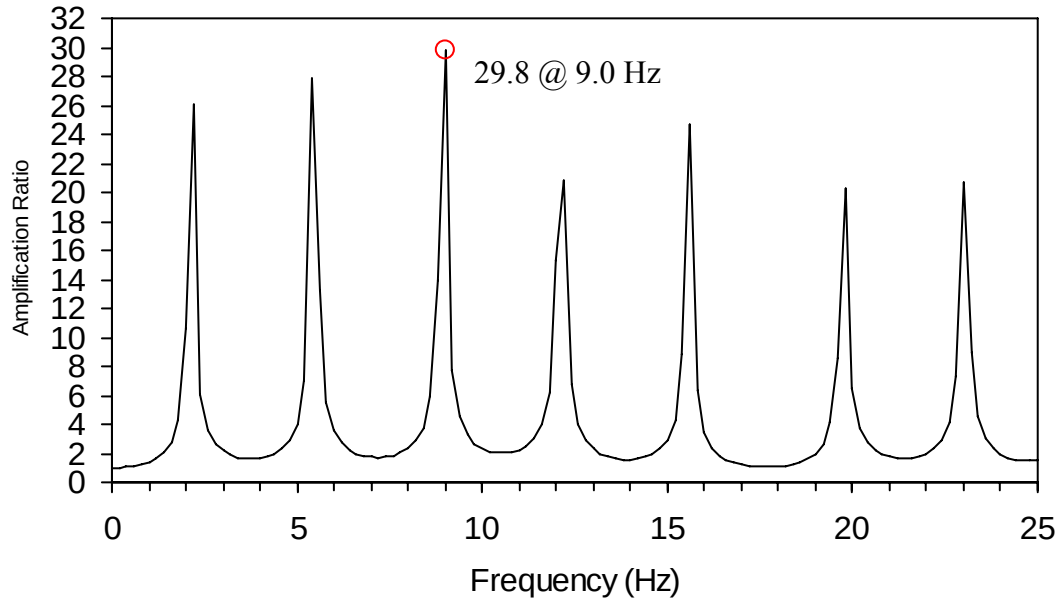

Figure B-8. VSAP M3.9 Ridgely, Tenn. longitudinal sensor transfer function.

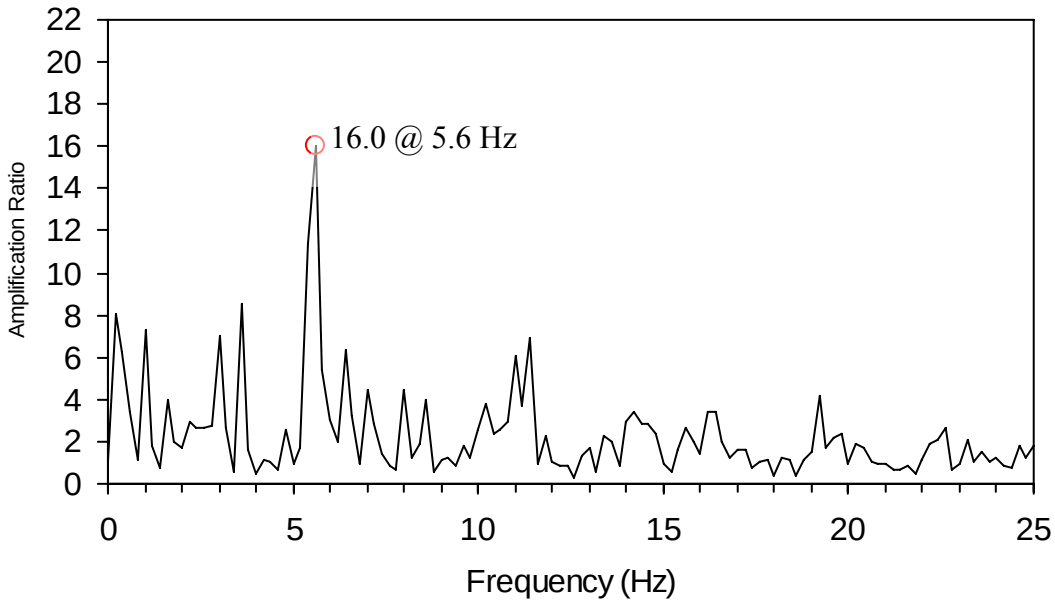

Figure B-9. VSAS M3.9 Ridgely, Tenn. transverse sensor transfer function.

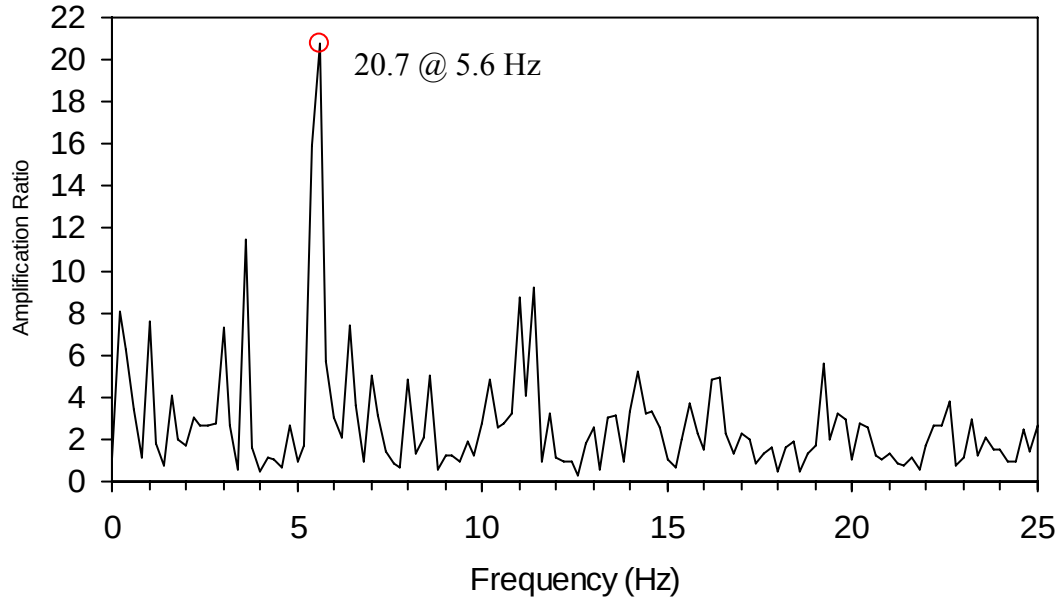

Figure B-10. VSAS M3.9 Ridgely, Tenn. longitudinal sensor transfer function.

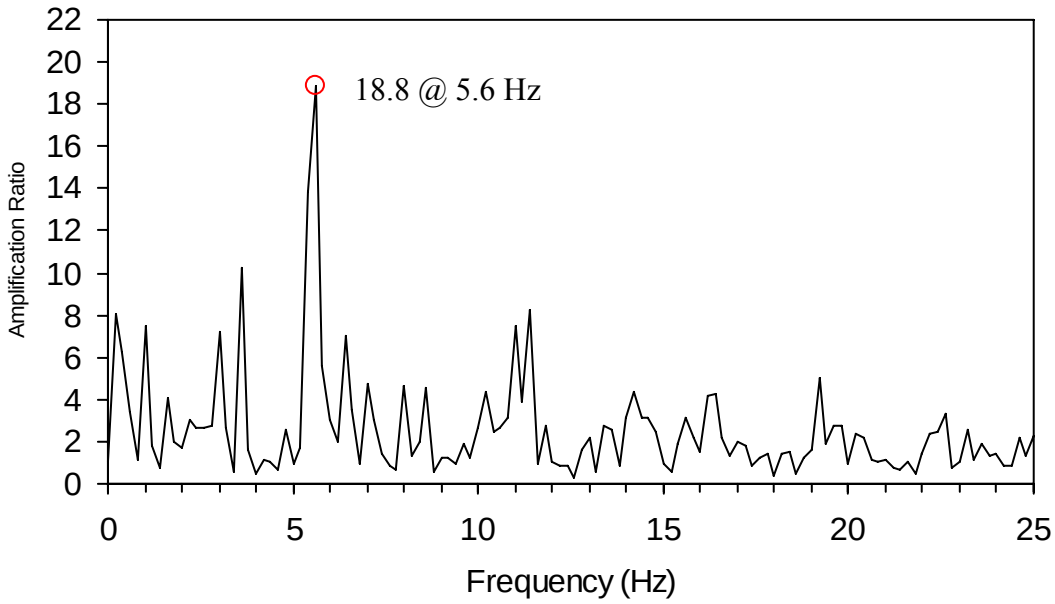

Figure B-11. VSAS M4.1 Arkansas transverse sensor transfer function.

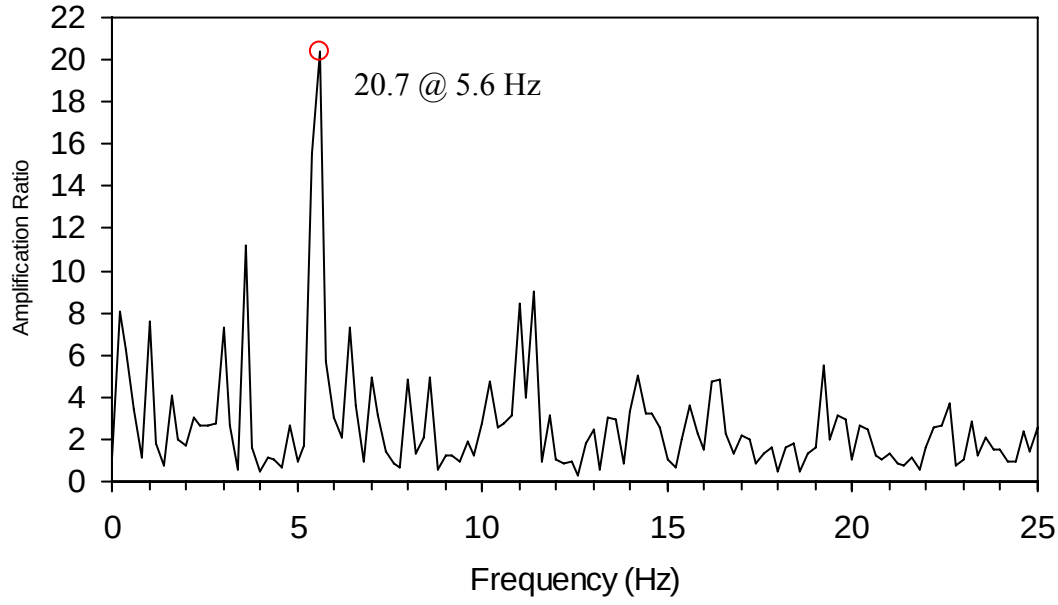

Figure B-12. VSAS M4.1 Arkansas longitudinal sensor transfer function.

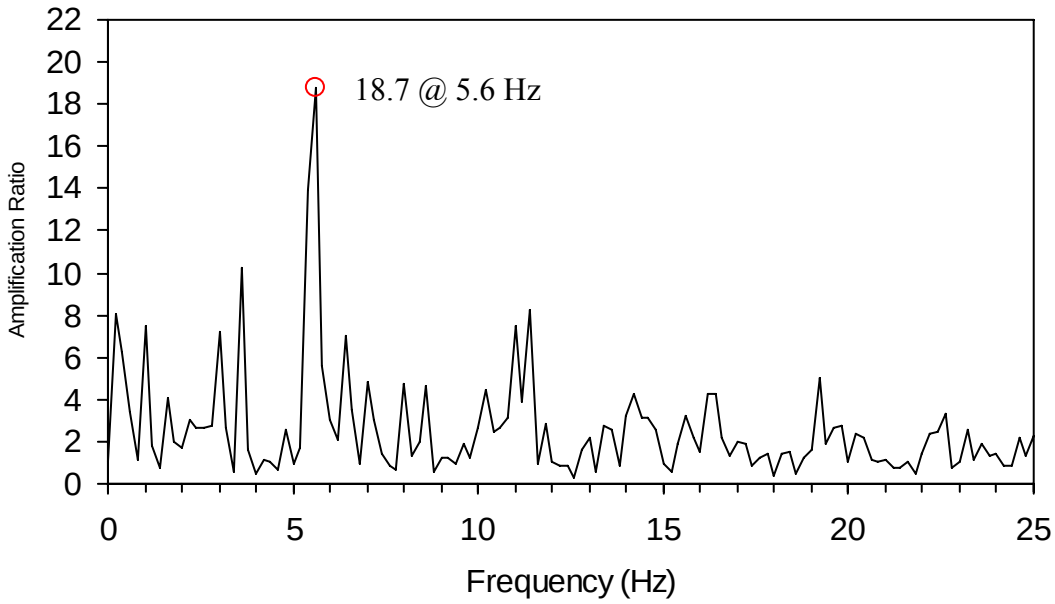

Figure B-13. VSAS M3.6 Blandville, Ky. transverse sensor transfer function.

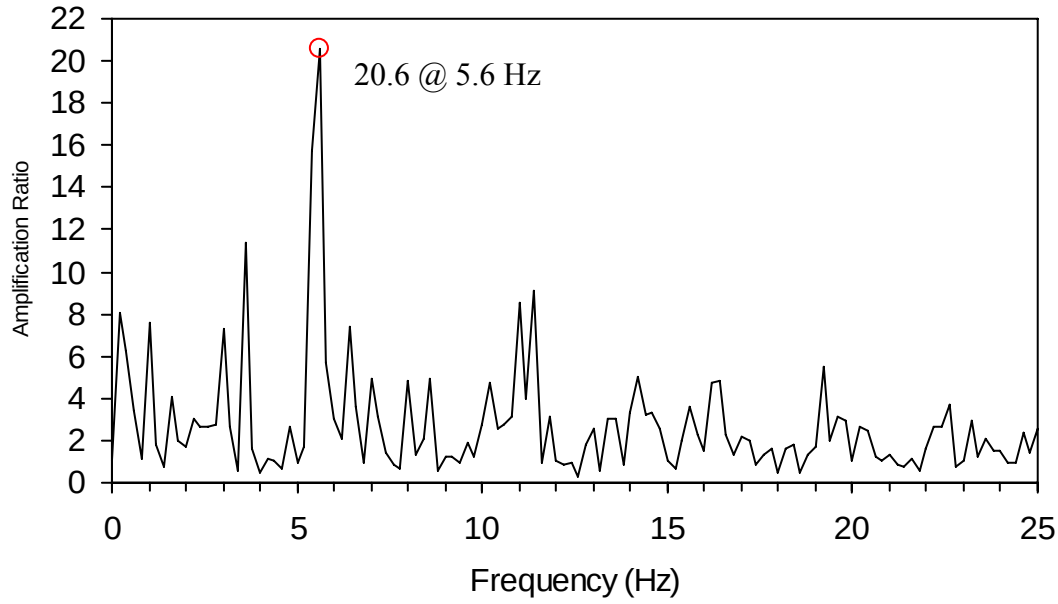

Figure B-14. VSAS M3.6 Blandville, Ky. longitudinal sensor transfer function.

CHAPTER SEVEN

7. REFERENCES CITED

Bakun, W.H., A.C. Johnston, and M.G. Hopper (2003). Estimating Locations and Magnitudes of Earthquakes in Eastern North America From Modified Mercalli Intensities, *Bulletin of the Seismological Society of America*, **93**, 190–202.

Bardet, J.P., K. Ichii, and C.H. Lin (2000). User's manual for EERA: A computer program for Equivalent-linear Earthquake site Response Analysis. Department of Civil Engineering, University of Southern California, Los Angeles, 40 p.

Clausen, J.L., J.W. Douthitt, K.R. Davis, and N.E. Phillips (1992). *Report of the Paducah Gaseous Diffusion Plant groundwater investigation phase III*. Report KY/E-150, prepared for the U.S. Department of Energy under contract no. DE-AC05-76OR00001, Paducah, Ky., Martin Marietta Energy Systems, Inc..

Hanson, R.D., R. Anderson, G.A. Bollinger, R. Dobry, J. Huang, and D.B. Ward (1980). Reconnaissance report-Northern Kentucky Earthquake of July 27, 1980, *Earthquake Engineering Research Institute Reconnaissance Report*, September, 1980, 105 p.

Harris, J. B. (1992). *Site Amplifications of Seismic Ground Motions in the Paducah, Kentucky, Area*: Lexington, University of Kentucky, PhD Dissertation.

Idriss, I.M. and J. Sun (1991). User's manual for SHAKE91. Center for Geotechnical Modeling, Department of Civil and Environmental Engineering, University of California, Davis,

Idriss, I. M., and H.B Seed (1968) Seismic response of horizontal soil layers, *Journal of Soil Mechanics and Foundation Engineering*, **94**, 1003–1031.

Johnston, A.C., and E.S. Schweig (1996). The enigma of the New Madrid earthquakes of 1811-1812, *Annual Review of Earth and Planetary Sciences*, **24**, 339–384.

Kramer, S.L. (1996). Geotechnical earthquake engineering, Upper Saddle River, N.J., Prentice Hall, 653 p.

Lin, T.L. (2003). *Local Soil-Induced Amplification of Strong Ground Motion in Maysville, Kentucky*, Lexington, University of Kentucky, M.S. Thesis.

Nuttli, O.W. (1973). The Mississippi Valley earthquakes of 1811-1812: Intensities, ground motion, and magnitude, *Bulletin of the Seismological Society of America*, **63**, 227–248.

Science Applications International Corporation (2002). *Seismic investigation report for siting a potential on-site CERCLA waste disposal facility at the Paducah Gaseous Diffusion Plant, Paducah, Kentucky*. DOE/OR.07-2038&D1, prepared for the U.S. Department of Energy under contract no. DE-AC05-98OR22700, Paducah, Ky. Bechtel Jacobs Company Inc.

Schanbel, P.B., J. Lysmer, and H.B. Seed (1972). SHAKE: A computer program for earthquake response analysis of horizontally layered sites. Earthquake Engineering Research Center, Report No. UCB/EERC72/12, University of California, Berkeley, 102 p.

Seed, H.B., and I.M. Idriss (1970). Soil moduli and damping factors for dynamic response analyses, Report no. EERC 70-10, Earthquake Engineering Research Center, University of California Berkeley.

Singh, S. K., E. Mena, and R. Castro (1988). Some aspects of source characteristics of the 19 September 1985 Michoacan earthquake and ground motion amplification in and near Mexico City from strong motion data, *Bulletin of the Seismological Society of America*, **78**, 451–477.

Street, R., and Z. Wang (2003). *Analysis of strong-motion records from the University of Kentucky accelerometers in the New Madrid Seismic Zone: 1990 through 2001:* Final report prepared for the U.S. Geological Survey, NEHRP Award 02HQGR0101, 7 p.

Street, R., Z. Wang, E. Woolery, J. Hunt, and J. Harris (1997). Site effects at a vertical accelerometer array near Paducah, Kentucky, *Engineering Geology*, **46**, 349–367.

Street, R., A. Zekulin, D. Jones, and G. Min (1988). A preliminary report on the variability in particle velocity recordings of the June 10, 1987, southeastern Illinois, earthquake, *Seismological Research Letters*, **59**, 89–97.

Tuttle, M.P., E. S. Schweig, J. D. Sims, R.H. Lafferty, L.W. Wolf, and M. L. Haynes (2002). The earthquake potential of the New Madrid Seismic Zone, *Bulletin of the Seismological Society of America*, **92**, 2080–2089.

Wang, Z., and E.W. Woolery (2006). Recordings from the Deepest Borehole in the New Madrid Seismic Zone, *Seismological Research Letters*, **77**, 148–153.

Wang, Z., E.W. Woolery, and J.A. Schaeffer (2003). A Short Note on Ground-Motion Recordings from the June 18, 2002, Darmstadt, Ind., Earthquake, *Seismological Research Letters*, **72**, 148–152.

Woolery, E.W., and Z. Wang (2005) *Seismic velocity measurements at expanded network sites*, Kentucky Research Consortium Energy and Environment Final Technical Report 04-72204a, 12p.

Woolery, E.W., and Z. Wang (2002). *A comprehensive geotechnical investigation and installation of a borehole accelerometer array in the New Madrid Seismic Zone*; Final report prepared for the U.S. Geological Survey, NEHRP Award 02HQGR0101, 13 p.

Yule, D.E., and R.E. Wahl (1996). User's manual for WESHAKE6. Waterways Experiment Station, Corps of Engineers, Department of the Army, Vicksburg, Mississippi.

Zhang, M., R. Street, J. Harris, and V.P. Drnevich (1993). A note on the influence of site conditions on ground motion values observed for the southeastern Illinois earthquake of June 10, 1987, *Seismological Research Letters*, **64**, 149–156.

Vita

- Born 3-12-75 in Hazard, KY
- University of Kentucky, Bachelors of Science: Geological Sciences,
- Jonathan Larry McIntyre, 12-12-08